RESEARCH ARTICLE

BIG enhances Arg/N-degron pathway-mediated protein degradation to regulate Arabidopsis hypoxia responses and suberin deposition

Hongtao Zhang[1], Chelsea Rundle[1], Nikola Winter[2], Alexandra Miricescu[3], Brian C. Mooney[3], Andreas Bachmair[2], Emmanuelle Graciet[3], Frederica L. Theodoulou[1]*

1. Plant Sciences and the Bioeconomy, Rothamsted Research, Harpenden, AL5 2JQ, UK
2. Department of Biochemistry and Cell Biology, Max Perutz Labs, University of Vienna, Vienna, Austria.
3. Department of Biology, Maynooth University, Maynooth, Ireland
Present address: AM: Pesticide Registration Division, Department of Agriculture, Food and the Marine, Backweston Campus, Celbridge, Co. Kildare, W23X 3PH, Ireland ; BCM: Department of Biology, University of Oxford, OX1 3RB, UK.

Short title: BIG enhances Arg/N-degron pathway-mediated protein degradation

One-sentence summary: The large protein BIG participates in the Arg/N-degron pathways to regulate hypoxia responses and broader functions in *Arabidopsis thaliana*.

* Corresponding author: Frederica L. Theodoulou (freddie.theodoulou@rothamsted.ac.uk)

The author responsible for distribution of materials integral to the findings presented in this article in accordance with the policy described in the Instructions for Authors (https://academic.oup.com/plcell/pages/General-Instructions) is: Frederica L. Theodoulou (freddie.theodoulou@rothamsted.ac.uk).

Abstract

BIG/DARK OVEREXPRESSION OF CAB1/TRANSPORT INHIBITOR RESPONSE3 is a 0.5-MDa protein associated with multiple functions in Arabidopsis (*Arabidopsis thaliana*) signalling and development. However, the biochemical functions of BIG are unknown. We investigated a role for BIG in the Arg/N-degron pathways, in which substrate protein fate is influenced by the N-terminal (Nt) residue. We crossed a *big* loss-of-function allele to two N-degron pathway E3 ligase mutants, *proteolysis6* (*prt6*) and *prt1*, and examined the stability of protein substrates. Stability of model substrates was enhanced in *prt6-1 big-2* and *prt1-1 big-2* relative to the respective single mutants and the abundance of the PRT6 physiological substrates, HYPOXIA-RESPONSIVE ERF2 (HRE2) and VERNALIZATION2 (VRN2) was similarly increased in *prt6 big* double mutants. Hypoxia marker expression was enhanced in *prt6 big* double mutants; this constitutive response required arginyltransferase activity and RAP-type ERFVII transcription factors. Transcriptomic analysis of roots not only demonstrated increased expression of multiple hypoxia-responsive genes in the double mutant relative to *prt6*, but also revealed other roles for PRT6 and BIG, including regulation of suberin deposition through both ERFVII-dependent and independent mechanisms, respectively. Our results show that BIG acts together with PRT6 to regulate the hypoxia response and broader processes in Arabidopsis.

Introduction

Targeted protein degradation is an important proteostatic mechanism that influences a multitude of agronomically important traits in plants (Linden and Callis, 2020; Theodoulou et al., 2022) and represents a major target for drug development in humans (Ciechanover, 2013; Kannt and Đikić, 2021). The Arg/N-degron pathways (formerly known as the Arg/N-end rule pathways) constitute a specialised form of proteostasis in which the N-terminal (Nt) residue of a given protein is the key determinant of a degradation signal, known as an N-degron (Bachmair et al., 1986; Varshavsky, 2019). N-degrons are revealed by protein cleavage by non-processive endopeptidases and/or created by subsequent enzymatic modification of the neo-N-terminus by amidases and arginyl tRNA transferase enzymes (ATEs) (Fig. 1A). In mammals and yeast, N-degrons include type 1 positively charged residues (Arg, Lys, His) and type 2 bulky hydrophobic residues (Trp, Phe, Tyr, Leu, and Ile), which are recognised by proteins known as N-recognins that facilitate substrate degradation.

The prototypical N-recognin, ubiquitin amino-end recognising protein 1 (Ubr1) of Baker's yeast (*Saccharomyces cerevisiae*) accepts both type 1 and type 2 substrates, whereas in mammals, four N-recognins, UBR1, UBR2, UBR4 and UBR5, which share a conserved UBR box domain, act semi-redundantly to mediate proteasomal and autophagic degradation of Arg/N-degron pathway substrates (Tasaki et al., 2005; 2009; 2013). In contrast, plants contain N-recognins with discrete substrate specificities (Garzón et al., 2007). PROTEOLYSIS6 (PRT6), the Arabidopsis (*Arabidopsis thaliana*) homologue of yeast Ubr1 and mammalian UBR1/2, is a candidate E3 ligase with specificity for basic N-termini (Arg, Lys, His), and PROTEOLYSIS1 (PRT1) is an unrelated ZZ domain protein with E3 ligase activity towards protein substrates bearing aromatic N-termini (Phe, Tyr, Trp) (Garzón et al., 2007; Potuschak et al., 1998; Stary et al., 2003; Graciet et al., 2010; Mot et al., 2018). Experimental evidence indicates the existence of a further (still unknown) N-recognin class that targets bulky/hydrophobic-N-termini (Leu and Ile) (Garzón et al., 2007; Graciet et al., 2010).

The availability of mutants and transgenics in which N-recognin function is disrupted has revealed diverse functions for the Arg/N-degron pathway in plants (Holdsworth

et al., 2020). Relatively little is known regarding the PRT1/N-degron pathway, although it has been shown to influence defence responses (de Marchi et al., 2016; Till et al., 2019) and the turnover of the E3 ligase BIG BROTHER (Dong et al., 2017). In contrast, the PRT6/N-degron pathway plays multiple roles in development (Yoshida et al., 2002; Choy et al. 2008; Holman et al., 2009; Graciet et al., 2009; Gibbs et al., 2014; Abbas et al., 2015; Zhang et al., 2018a,b; Gibbs et al., 2018; Weits et al., 2019; Labandera et al., 2021), plant–pathogen interactions (de Marchi et al., 2016; Gravot et al., 2016; Vicente et al., 2019), and responses to the abiotic environment (Gibbs et al., 2011; Licausi et al., 2011; Abbas et al., 2015; Weits et al., 2014; Mendiondo et al., 2016; Vicente et al., 2017; Hartman et al., 2019; Lamichhane et al., 2020; Lou et al., 2022; Abbas et al., 2022).

The first substrates of the PRT6/N-degron pathway were identified in the context of oxygen sensing (Gibbs et al., 2011; Licausi et al., 2011). Arabidopsis has five Group VII ethylene response factor transcription factors (ERFVIIs) bearing a conserved cysteine residue at position two, of which *RELATED TO APETALA (RAP) 2.12*, *RAP2.2*, and *RAP2.3* are constitutively expressed, whereas *HYPOXIA RESPONSIVE ERF* (*HRE*) *1* and *HRE2* are induced by low oxygen (Licausi et al., 2010). All five Met-Cys-ERFVII proteins undergo co-translational Nt Met excision to reveal Nt Cys, which under normoxia is susceptible to oxidation by PLANT CYSTEINE OXIDASE (PCO) enzymes and subsequent arginylation by ATEs (Weits et al., 2014; White et al., 2017). N-terminally arginylated ERFVIIs are then thought to be recognised by PRT6, which targets the proteins for proteasomal degradation (Gibbs et al., 2011; Licausi et al., 2011). However, when oxygen is limiting, ERFVIIs are stabilised and co-ordinate the transcriptional response to hypoxia. Consequently, hypoxia responsive genes, such as *ALCOHOL DEHYDROGENASE* (*ADH*) and *PHYTOGLOBIN1* (*PGB1*) (as well as *HRE1* and *HRE2*) are ectopically expressed in *prt6* alleles (Choy et al., 2008; Gibbs et al., 2011; Riber et al., 2015). The Arabidopsis genome encodes 248 Met-Cys initiating proteins, of which the polycomb repressive complex 2 subunit, VERNALIZATION 2 (VRN2) and the transcription factor LITTLE ZIPPER 2 (ZPR2) have also been confirmed as oxygen-sensitive physiological PRT6/N-degron pathway substrates with roles in development (Gibbs et al., 2018; Labandera et al., 2021; Weits et al., 2019).

Experimental evidence and sequence database searches indicate that the full suite of N-recognins has not yet been identified in plants (Garzón et al., 2007; Graciet et al., 2010). Arabidopsis has three UBR box proteins: PRT6, BIG (also known as DARK OVEREXPRESSION OF CAB1; DOC1 and TRANSPORT INHIBITOR RESPONSE3; TIR3), and AT4G23860 (Tasaki et al., 2005). Here, we investigated a potential role for BIG in the Arg/N-degron pathways, since its mammalian and Drosophila (*Drosophila melanogaster*) homologues (UBR4 and Calossin/Pushover, respectively) are known N-recognins (Tasaki et al., 2005; 2009; Ashton-Beaucage et al., 2016; Yoo et al., 2018; Hunt et al., 2019). Beyond the N-degron pathway, UBR4 has been implicated in proteasomal, autophagosomal and lysosomal degradation of cytoplasmic and membrane proteins (Tasaki et al., 2013; Lin et al., 2013; Hong et al., 2015; Kim et al., 2018; Hunt et al., 2019) and contributes to protein quality control (Yau et al., 2017; Tang et al., 2020; Hunt et al., 2021). UBR4 interacts with E3 ligases of different classes (Ashton-Beaucage et al., 2016; Yau et al., 2017; Hunt et al., 2019) and is also proposed to be an E3 ligase, largely based on genetic evidence. However, only relatively recently has its E3 ligase activity been characterised biochemically (Yau et al., 2017; Hunt et al., 2019; Tang et al. 2020), and shown to require a non-canonical hemi-RING domain, that is conserved in BIG (Barnsby-Greer et al., 2024).

BIG has been identified in around twenty different forward genetic screens and associated with diverse physiological functions via reverse genetics in Arabidopsis. The first *big* allele, *dark overexpression of CAB* (*doc1-1*), was isolated in a screen for mutants with mis-regulated photosynthetic gene expression (Li et al., 1994). *doc1-1,* which displays a striking morphological phenotype of reduced apical dominance and small stature, was subsequently found to be allelic to *transport inhibitor response3* (*tir3-1*), a mutant compromised in auxin transport (Ruegger et al., 1998; Gil et al., 2001). The affected gene was identified via map-based cloning and renamed in recognition of its exceptional size: *BIG,* which is expressed throughout the plant, encodes a 5077 amino acid protein with a predicted molecular weight of 565,597 Da (Gil et al., 2001; He et al., 2018). *BIG* was later shown to influence multiple hormone signalling pathways and different aspects of plant development (Kanyuka et al., 2003; Desgagné-Penix et al., 2005; Yamaguchi et al., 2007; 2013; Guo et al., 2013; Shinohara et al., 2013; Zhang et al., 2020; Liu et al., 2022). Recent studies indicate

further, apparently disparate functions for *BIG* in the circadian clock, guard cell signalling, calcium homeostasis, regulation of C/N balance, response to pathogens, cell death, and wound-induced rooting (Üstün et al., 2016; Meitignier et al., 2017; He et al., 2018; Hearn et al., 2018; Zhang et al., 2019a,b; Bruggeman et al., 2020; Modrego et al., 2023). Although many *big* mutant phenotypes can be ascribed to dysregulation of auxin transport (Li et al., 1994; Ruegger et al., 1998; Gil et al., 2001; López-Bucio et al., 2005; Kasajima et al., 2007; Yamaguchi et al., 2007; 2013; Guo et al., 2013; Ivanova et al., 2014; Wu et al., 2015; Zhang et al., 2020), this is not the case for all processes influenced by BIG and to date its precise biochemical functions have remained unclear.

In this study, we demonstrate that BIG participates in the Arg/N-degron pathways, acting semi-redundantly with PRT6 and PRT1. PRT6/N-degron pathway substrates hyperaccumulate in *prt6 big* double mutants, enhancing the molecular response to hypoxia in an ERFVII-dependent fashion. This was confirmed by RNA-seq analysis which also indicated a range of different genetic interactions between *big-2* and *prt6-5* that influence transcription of additional groups of genes, pointing to broader functions for BIG and PRT6, including the regulation of suberin deposition.

Results

BIG influences the stability of model Arg/N-degron pathway substrates

To test whether BIG plays a role in the Arg/N-degron pathways, we used the ubiquitin fusion technique to produce pathway substrates *in planta* (Varshavsky, 2000). We took advantage of the DHFR-Ub-X-GUS system (Garzón et al., 2007), in which a genetically encoded ubiquitin domain is cleaved *in vivo* by deubiquitinating enzymes to produce a reporter protein, β-glucuronidase (GUS) bearing a residue of choice (X) at the N-terminus, and a stable reference protein, dihydrofolate reductase (DHFR) (Fig. 1B). Lines expressing constructs designed to release a type 1, basic Nt substrate (R-GUS), a type 2, aromatic Nt substrate (F-GUS), and a stable control (M-GUS) were generated in the wild-type Arabidopsis accession, Columbia-0 (Col-0), and in different mutant backgrounds lacking known N-recognins and *BIG*. Details of

the *big-2* allele used in this study and originally described in (Kasajima et al., 2007) are provided in Supplementary Fig. 1 and Supplementary Table 1.

The stability of X-GUS was assessed by immunoblotting and histochemical staining. Immunoblotting revealed that the fusion proteins were cleaved as predicted and that R-GUS and F-GUS were unstable in Col-0 wild type seedlings, relative to the DHFR control (Fig. 1C;). R-GUS and F-GUS were stabilised in *prt6-1* and *prt1-1* mutants, respectively, as previously reported (Garzón et al., 2007; Zhang et al., 2018a). In contrast, M-GUS was stable in all backgrounds tested (Fig 1C, D). R- and F-GUS reporters were not stabilised in the *big-2* single mutant, but stability of R-GUS was enhanced in the *prt6-1 big-2* double mutant compared to *prt6-1* (Fig. 1E). Similarly, F-GUS was more stable in *prt1-1 big-2* than in *prt1-1* (Fig. 1F). Histochemical staining for GUS activity was consistent with these results (Fig. 1G). Together, these data indicate that BIG acts together with known N-recognins to mediate the degradation of substrates initiating with R and F. As an independent test, a cleavable R-luciferase (R-LUC) reporter (Worley et al., 2000; Graciet et al., 2010) was also introduced into *prt6-5 big-2* (Supplementary Fig. 2A). R-LUC was unstable in Col-0 and *big-2* but detected in both *prt6-5* and *prt6-5 big-2*, with higher luciferase activity in the double mutant, consistent with enhanced stabilisation of the R-LUC protein in *prt6-5 big-2* (Supplementary Fig. 2B).

To complement the genetic approach, potential protein interactions with N-degrons were investigated using proximity labelling (Mair et al., 2019). Transgenic lines expressing a modified *Escherichia coli* biotin ligase (TurboID)-YFP fusion designed to reveal either an Nt M- or R- residue (Fig. 2A) were generated in the Col-0 background. Proteins biotinylated by the Turbo-ID fusions were enriched on streptavidin beads (Fig. 2B) and analysed by mass spectrometry. Both PRT6 and BIG were enriched in the R-TurboID sample relative to the M-TurboID sample, indicating their proximity to R-TurboID *in planta*, and suggesting a potential physical interaction of Nt Arg residues with PRT6 and BIG (Fig. 2C). Interestingly, regulatory proteasomal subunits and Homologous to E6AP C-terminus (HECT) ubiquitin E3 ligases known to be associated with the proteasome (Wang and Spoel, 2022) were also highly enriched in the R-TurboID sample (Fig. 2C; Supplementary Data Set 1).

BIG influences the abundance of physiological PRT6/N-degron pathway substrates

To explore whether BIG influences the stability of physiological substrates, we focused on the PRT6/N-degron pathway, for which several targets have been identified. We first tested two representative ERFVII transcription factors by crossing plants expressing HA-tagged HRE2 and RAP2.3 (Pro35S:HRE2-HA, Gibbs et al., 2011; Pro35S:RAP2.3, Gibbs et al., 2014) to N-degron pathway mutants and *big-2*. The protein abundance of HRE2-HA was increased in *prt6-5 big-2* roots relative to the single *prt6-5* mutant (Fig. 3A). Transgene-specific RT-qPCR showed that the increased levels of HRE2-HA protein were not driven by an increase in transcript abundance (Fig. 3B).

Consistent with the known role of ERFVIIs in inducing hypoxia responsive gene expression, the enhanced HRE2-HA protein abundance in *prt6-5 big-2* relative to *prt6-5* was accompanied by a much stronger induction of the core hypoxia genes *ALCOHOL DEHYDROGENASE* (*ADH*) and *PHYTOGLOBIN1* (*PGB1*) and the respective proteins (Fig. 3A, C). RAP2.3-HA protein was stable in *prt6-5* seedlings, but not detectable in Col-0 and *big-2* (Fig. 3D) and hypoxia markers were strongly enhanced in the *prt6-5* line (Fig. 3D, F). Transgene transcript levels of *RAP2.3* were lower in the *prt6-5* background compared to Col-0, indicating that the increased abundance of RAP2.3-HA is due to post-transcriptional regulation (Fig. 3E).

prt6-5 seedlings expressing Pro35S:RAP2.3-HA had curled cotyledons with a defective cuticle and the true leaves developed more slowly (Supplementary Fig. 3A, B); rosette development and flowering were also delayed (Supplementary Fig. 4A, B). *prt6-5 big-2* double mutant lines expressing Pro35S:RAP2.3-HA exhibited curled leaves and generally stunted growth, and flowering was extremely delayed with only a short primary bolt produced (Supplementary Fig. 4B). We were unable to recover seeds from these plants*;* dissection of flowers revealed incompletely elongated stamens that did not mature or release pollen (Supplementary Fig. 4C). Therefore, we analysed pooled seedlings homozygous for *prt6-5* but segregating for *big-2*. Accordingly, we observed a modest increase in RAP2.3-HA abundance and hypoxia marker expression, despite only one quarter of these seedlings being homozygous for both mutations (Fig. 3G).

We next tested whether the abundance of a functionally distinct endogenous N-degron pathway substrate, VRN2, was influenced by BIG, using a VRN2-GUS fusion

driven by the native *VRN2* promoter (ProVRN2:VRN2-GUS; Gibbs et al., 2018). Histochemical staining confirmed previous results (Gibbs et al., 2018) with GUS present throughout the seedling in the *prt6-1* background, and additionally revealed increased intensity in *prt6-1 big-2* relative to *prt6-1* (Fig. 3H). Immunoblotting showed specifically that VRN2-GUS was increased in abundance in *prt6-1 big-2* compared to *prt6-1* and unstable in Col-0 and *big-2* (Fig. 3I). RT-qPCR demonstrated that there were no significant differences in *VRN2 or GUS* expression between *prt6-1* and *prt6-1 big-2*, indicating that changes in VRN2-GUS abundance relate to post-translational control by PRT6 and BIG (Fig. 3J).

BIG works in parallel with PRT6 to regulate the hypoxia response

To further understand how BIG regulates the hypoxia response, we constructed a series of combination mutants using alleles lacking pathway substrates and enzymes, and then quantified hypoxia markers. Firstly, to observe whether arginylation is necessary for BIG to participate in the N-degron pathway, a mutant lacking arginyl transferase activity was crossed to *big-2*. Expression of *ADH* and *PGB1* and accumulation of the respective proteins were comparable in *ate1 ate2* and *ate1 ate2 big-2*, indicating that regulation of the hypoxia response by *BIG* is dependent on arginylation (Fig. 4A, B). Genetic removal of *RAP2.12*, *RAP2.2* and *RAP2.3* was sufficient to prevent constitutive expression of hypoxia markers in *prt6-1* seedlings, as shown previously (Zhang et al., 2018a), and also in the *prt6-1 big-2* background (Fig. 4C, D) demonstrating that BIG influences hypoxia gene expression exclusively through RAP-type ERFVIIs. The mutants were also followed through development to determine whether regulation of ERVIIs underpins other phenotypes of *prt6-1 big-2*. Removal of RAP-type ERFVIIs did not have an impact on the overall morphology of *big-2*, consistent with the lack of stabilisation in the single mutant. However, the stunted size and delayed flowering of *prt6-1 big-2* was partially rescued by removal of these substrates (Supplementary Fig. 5).

Given that the increased stabilisation of ERFVII transcription factors in *prt6-1 big-2* was associated with enhanced levels of key hypoxia response genes and proteins (Fig. 3, Fig. 4), we hypothesised that the double mutant might be more tolerant of hypoxia than *prt6*. Chlorophyll retention can be used as a marker of hypoxia tolerance, and we found that *prt6-1 big-2* and *prt6-5 big-2* seedlings had enhanced

chlorophyll levels compared to the respective single mutants following hypoxia treatment, but similar seedling survival rates (Supplementary Fig. 6A-D). Ectopic expression of RAP2.3 in *prt6-5*, where *ADH* levels were markedly elevated, dramatically enhanced both chlorophyll content and survival of seedlings following hypoxia (Supplementary Fig. 6E-G), consistent with the role of RAP2.3 as a positive regulator of hypoxia responses. We also tested two further, distinct types of hypoxia response: primary root regrowth after hypoxia treatment (in seedlings) and waterlogging tolerance (in mature plants). We did not observe reproducible tolerance of *prt6* or *prt6 big-2* mutants in root re-growth assays, but ~20 % of *prt6-5* roots expressing Pro53S:RAP2.3-HA re-grew after 4 h hypoxia (Supplementary Fig. 7A). Although *prt6* alleles exhibited waterlogging tolerance, *big-2* and *prt6 big-2* plants were sensitive to waterlogging, presumably due to their greatly reduced root system. Interestingly, ectopic expression of RAP2.3-HA did not confer waterlogging tolerance under the conditions tested (Supplementary Fig. 7B).

VRN2 was first defined as a key regulator of vernalisation, but also contributes to hypoxia stress survival, with the *prt6-1 vrn2-5* mutant exhibiting lower tolerance than *prt6-1* (Gibbs et al., 2018). However, *VRN2* was not required for hypoxia gene expression, indeed, expression of *PGB1* was increased in *prt6-1 vrn2-5* compared to *prt6-1* (Fig. 4E, F), suggesting that VRN2 may suppress expression of some hypoxia responsive genes under conditions where ERFVIIs are stabilised. Other hypoxia responsive genes (*ADH1*, *ACC OXIDASE 1*, *HYPOXIA RESPONSE ATTENUATOR1*, *HYPOXIA RESPONSE UNKNOWN PROTEIN 40*, *PCO1*, *PCO2*, *PYRUVATE DECARBOXYLASE-2*) followed a similar trend but it was not statistically significant (Supplementary Fig. 8).

The root transcriptome is extensively remodelled in *prt6-5 big-2* mutants

To obtain further insight into the impact of *BIG* on the PRT6/N-degron pathway and potentially other processes, we conducted mRNA sequencing (RNA-seq) analysis of *big-2*, *prt6-5*, *prt6-5 big-2* and Col-0 roots. One-centimetre root sections containing the root tip were selected to minimise potential developmental effects associated with the small size of *big-2* seedlings. As principal component analysis indicated that samples clustered tightly by genotype (Supplementary Fig. 9A), we generated lists of differentially expressed genes (DEGs) for each mutant relative to wild-type, with a

cut-off fold-change of 2 and adjusted p-value<0.01 (Supplementary Data Set 2). Analysis of DEGs identified 92 and 119 genes up-regulated in *prt6-5* and *big-2*, respectively, with only 16 common DEGs. 341 and 438 genes were down regulated in *prt6-5* and *big-2*, respectively, with 186 common to both data sets (Fig. 5A). Greater numbers of DEGs were identified in *prt6-5 big-2* and in many cases the fold changes of the common DEGs were markedly elevated in the double compared to the respective single mutants (Fig. 5B), indicative of a genetic interaction between *prt6-5* and *big-2*. There were notable overlaps between genes up regulated in *prt6-5* and *prt6-5 big-2* roots with previously published microarray data from *prt6* and *ate1/2* seedlings (Gibbs et al., 2011; de Marchi et al., 2016), but little overlap between *big-2* DEGs and the published data for *prt6* and *ate1/2* (Supplementary Fig. 9B-D).

Gene ontology (GO) term analysis (Ge et al., 2020) for “Biological Process” revealed that hypoxia-related terms were highly enriched in *prt6-5* and *prt6-5 big-2* up regulated genes, whereas “Photosynthesis”, “Glycolate and dicarboxylate metabolism” and “Carbon metabolism” were enriched in *big-2* up regulated DEGs (Supplementary Fig. 10). All the 49 “core” genes known to be induced across cell types by hypoxia in wild-type plants (Mustroph et al., 2009) were present in the full transcriptome data set, with 21 up regulated in *prt6-5*. Comparison with transcriptome data from (Lee et al., 2011) revealed further hypoxia-responsive genes that are constitutively up regulated in *prt6-5* and *prt6-5 big-2* roots (Fig. 5C). In agreement with RT-qPCR and immunoblotting data (Fig. 4), the fold-change in expression was markedly enhanced in *prt6-5 big-2* relative to the *prt6-5* single mutant (Fig. 5D) indicating an enhancement that is consistent with the increased stability of N-degron substrates such as the ERFVIIs (Fig. 5E). Six of the seven known N-degron pathway substrates were represented in the RNA-seq data set, among which only the hypoxia-responsive genes *HRE1* and *HRE2* were up regulated in *prt6-5 big-2* (Supplementary Fig. 9E).

Suberin deposition is repressed in *prt6* and *big-2* roots

Of the down-regulated genes, “Glucosinolate biosynthetic process” was enriched in *prt6-5* and *prt6-5 big-2* DEGs, in agreement with previous findings for *ate1/2* (de Marchi et al., 2016) and “Cellular response to iron starvation” was enriched in *prt6-5* and *big-2* (Supplementary Fig. 11). Strikingly however, the most enriched terms for down-regulated genes in all genotypes were “Suberin biosynthetic process” and “Cutin

biosynthetic process", two pathways which share common components (Li-Beisson et al., 2013) (Supplementary Data Set 2). Genes associated with suberin biosynthesis and transport were down regulated in both *big-2* and *prt6-5*, accounting for almost all the steps in the pathway. These include long chain acyl-CoA synthetases, 3-ketoacyl CoA synthetases, fatty acid reductases, fatty acid omega-hydroxylases, glycerol acyltransferases, feruloyl acyltransferase, fatty alcohol caffeoyl-CoA transferase, 4-coumarate-CoA ligase, ABC transporters, lipid transfer proteins and GDSL lipases (Li-Beisson et al., 2013; Serra and Geldner, 2022). Fold changes of the differentially regulated genes were greater in *prt6-5 big-2*, compared to the respective single mutants (Fig. 6A; Supplementary Data Set 2).

Moreover, six MYB transcription factors (*MYB9*, *MYB41*, *MYB53*, *MYB52*, *MYB93* and *MYB39/SUBERMAN*) which act in a hierarchical network to control suberin biosynthesis in Arabidopsis (Shukla et al., 2021; Xu et al., 2022) are also down regulated in the N-degron pathway mutants, with fold-change increased in *prt6-5 big-2* relative to the single mutants (Supplementary Fig. 12A). In agreement with this, 45 of 149 genes up regulated in *AtMYB41*-overexpressing plants (Cominelli et al., 2008) were down-regulated in *prt6-5 big-2* (Supplementary Fig. 12B). RT-qPCR analysis showed that transcript levels of representative suberin genes were not significantly different between Col-0 and *prt6-1 rap2.12 rap 2.2 rap2.3*, indicating that their repression in *prt6-1* roots requires RAP-type ERFVII transcription factors. In contrast, repression of suberin genes in *big-2* roots was ERFVII-independent (Fig. 6B).

To explore the physiological significance of altered gene expression in the mutants, roots were stained with Fluorol Yellow 088. As *big-2* roots were significantly shorter than those of other genotypes (Supplementary Fig. 12C), suberization was expressed as a percentage of root length. The suberized zone was less extensive in *prt6-5*, *big-2*, and *prt6-5 big-2* roots than in wild type Col-0 roots (Fig. 6C, D; Supplementary Fig. 12D. Taken together, the results indicate that suberin deposition is constrained in PRT6/N-degron pathway mutant roots by ERFVII stabilisation, and via an additional mechanism in *big-2*, pointing to shared and distinct roles for *BIG* and *PRT6* in control of this process.

Subsequent to the transcriptome study, re-sequencing of the *big-2* mutant revealed a second T-DNA inserted in the final exon of At3g61680 (*PLASTID LIPASE 1*; *PLIP1*) which encodes a plastid localised phospholipase A1 involved in seed oil biosynthesis (Wang et al., 2017; Supplementary Fig. 1). We designated this allele

plip1-3 as two T-DNA mutants have been reported previously (Wang et al., 2017). *BIG* and *PLIP1* are located at opposite ends of chromosome 3 and consequently, in most cases, we were able to work with material in which the second T-DNA had been segregated out. An important exception is the RNA-seq analysis which unfortunately was performed with the seed homozygous for *plip1-3*. We consider it unlikely that a lesion in *PLIP1* would lead to stabilisation of N-degron pathway substrates. Nevertheless, to rule out the possibility that the lesion in *PLIP1* was causal for any of the *big-2* phenotypes reported in this paper, we repeated RT-qPCR analysis using material lacking *plip1-3*. This clearly demonstrated that the enhanced expression of hypoxia-responsive genes in *prt6-1 big-2* is independent of *plip1-3*, as is the altered expression of suberin genes (Supplementary Fig. 13). Whilst it is possible that *plip1-3* influences other transcript changes in *big-2* and *prt6-5 big-2*, we conclude that the key findings of the study (including those from the transcriptome data) are robust.

Discussion

Despite the physiological and agronomic importance of the plant Arg/N-degron pathways, not all of the molecular components have yet been identified (Holdsworth et al., 2020). The PRT6 N-recognin influences the stability of Type 1 substrates such as those initiating with R that can be generated by the action of protein cleavage and/or arginyl t-RNA protein transferase enzymes (ATEs) (Garzón et al., 2007; Graciet et al. 2009; Gibbs et al., 2011; Licausi et al., 2011; White et al., 2017). Notably however, incomplete stabilisation of the model substrate R-GUS in *Arabidopsis thaliana prt6* mutants (Garzón et al., 2007) and the more severe phenotype of *ate1 ate2* compared to *prt6* (Graciet et al. 2009) suggest the possibility of an additional N-recognin with specificity for PRT6/N-degrons. In this study, we provide several lines of evidence that the giant UBR box protein, BIG mediates turnover of proteins bearing type 1 N-degrons in concert with the PRT6/N-degron pathway and show that this influences the molecular response to low oxygen in Arabidopsis. Moreover, we demonstrate that BIG also contributes to the turnover of proteins with type 2 N-degrons via the PRT1/N-degron pathway.

This study utilised the *big-2* allele in which the T-DNA is inserted about halfway through the gene (Supplementary Fig. 1). As it has a severe morphological phenotype, we considered that *big-2* is likely to be a loss of function allele and our RNA-seq data indicate that *big-2* expresses a truncated transcript, albeit at a much lower level than wild type (Supplementary Dataset 2). Although the truncated transcript could potentially produce a protein containing the UBR box, it is unclear whether the truncated protein would be correctly folded. Importantly, information from Drosophila and mammalian homologues of BIG indicate that a truncated protein is likely to be non-functional in the N-degron pathway because it lacks the hemi-RING E3 ligase domain (Barnsby-Greer et al., 2024). In theory, a mutant allele that produces a truncated protein could be a dominant negative but plants heterozygous for *big-2* look similar to wild type suggesting that there is no dominant negative effect (Supplementary Fig. 1).

Using N-degron pathway reporters, we demonstrated enhanced stability of a model PRT6 substrate, R-GUS as well as increased abundance of R-LUC and physiological substrates, HRE2 and VRN2 in the *prt6-5 big-2* mutant relative to *prt6-5* (Fig. 1; Fig. 3; Supplementary Fig. 2). The increased abundance of HRE2 and VRN2 was not driven by increased transcript, thus, whilst we cannot rule out increased translation, the data are consistent with increased stability in the double mutant background, as shown for R-GUS. It was not possible to test unequivocally whether RAP2.3 is similarly stabilised in *prt6-5 big-2* seedlings since double mutant plants expressing Pro35S:RAP2.3-HA did not set seed (Supplementary Fig. 4). However, this observation, together with the partial rescue of delayed flowering and reduced fertility of *prt6-5 big-2* plants by genetic removal of *RAP* function (Supplementary Fig. 4) strongly suggests that RAP2.3 is also hyperstabilised in the double mutant and that extreme stabilisation of RAP-type ERFVII transcription factors is deleterious to growth and reproduction.

The vegetative phenotype of *prt6-5 big-2* lines expressing Pro35S:RAP2.3-HA resembles that of other plants in which N-degron pathway substrates are stabilised, including transgenics expressing N-terminally truncated RAP2.12 (Giuntoli et al., 2017) and mutiple *pco* mutants (Weits et al., 2022; Masson et al., 2019). Interestingly, constitutive expression of RAP2.3-HA in *prt6-5* did did not have a profound effect on morphology in mature plants, but development was considerably

delayed and seedlings exhibited curled cotyledons with a slight cuticle defect (Supplementary Fig. 3 and 4). This aligns with the observation of (Giuntoli et al., 2017) that, although the PRT6/N-degron pathway controls ERFVII stability throughout vegetative development, ERFVII-dependent transcriptional activation is attenuated with age.

Stabilisation of PRT6/N-degron pathway substrates in *prt6-5 big-2* plants markedly amplified the transcriptional response to hypoxia, as evidenced by RT-qPCR, immunoblot, and especially RNA-seq analysis, and was accompanied by enhanced chlorophyll retention in seedlings following hypoxia treatment (Fig. 3-5; Supplementary Fig. 6). Additional approaches to explore low oxygen tolerance were explored, however, it was challenging to associate increased expression of hypoxia responsive genes with hypoxia tolerance against a backdrop of a pleiotropic mutant phenotype. Primary root elongation and lateral root development are severely impaired in *big-2* (Ruegger et al., 1997; López-Bucio et al. 2005; Yamaguchi et al. 2007; Guo et al., 2013) and we ascribe the waterlogging sensitivity of *big-2* and *prt6 big-2* (Supplementary Fig. 7B) to their highly reduced root systems. Intriguingly, whilst over expression of RAP2.3 in *prt6-5* conferred hypoxia tolerance to seedlings in both chlorophyll retention and root regrowth assays, mature plants were intolerant of waterlogging under the conditions used. This could be explained by the aforementioned age dependent decline in the ability of ERFVIIs to modulate gene expression (Giuntoli et al., 2017). It is also possible that the small roots of these plants are unable to withstand longer periods of oxygen deprivation, whereas the acute stresses in the chlorophyll retention and root regrowth assays allow for a better comparison across genotypes.

Higher order combination mutants demonstrated that BIG and PRT6 control the hypoxia response in seedlings exclusively through RAP-type ERFVII transcription factors (Fig. 4C,D). Interestingly, however, stabilisation of the PRC2 subunit VRN2 in PRT6/N-degron pathway mutants negatively influenced expression of the hypoxia-responsive gene *PGB1* (Fig. 4E, F). The mechanism by which this occurs remains to be explored but may involve methylation, given the known role of the PRC2 complex in epigenetic regulation. We did not explore the impact of enhanced VRN2 stabilisation on flowering since the *big-2* allele is in the Col-0 background which does

not require vernalisation. Furthermore, ectopic expression of *VRN2* does not remove the requirement for vernalisation in ecotypes that require prolonged winter to initiate flowering (Labandera et al., 2021).

RNA-seq analysis revealed that BIG and PRT6 not only play a role in the hypoxia response but also influence the expression of several other groups of genes, particularly a regulon associated with suberin biosynthesis. Suberin is a complex polymer that can act as a barrier to nutrients and gases, and which shows remarkable developmental plasticity in roots (Shukla et al., 2021). *big-2* and *prt6-5* had an independent, partially additive negative effect on transcript abundance (Fig. 6A, B; Supplementary Fig. 12). In agreement with the lower expression of key *MYB* transcription factors and their downstream targets, suberin deposition was reduced in *big-2*, *prt6-5*, and *prt6-5 big-2* roots (Fig. 6C, D). *RAP2.12*, *2.2* and *2.3* were required for the repression of suberin biosynthetic genes in *prt6*, which is perhaps surprising given that limiting radial oxygen diffusion through suberin deposition is an adaptive response to waterlogging in wetland species (Ejiri et al., 2021). However, there are important temporal and developmental differences between wild type plants experiencing hypoxia in the field and Arabidopsis roots grown on plates; negative regulation of suberization by ERFVIIs may be a feedback mechanism triggered by the sustained activation of the hypoxia response in N-degron pathway mutants.

Intriguingly, repression of suberin biosynthetic genes in the *big-2* single mutant was independent of ERFVII transcription factors (Fig. 6B), suggesting that BIG influences other factors that control suberin deposition independently of PRT6. Suberization is strongly influenced by hormones, including auxin, which is associated with the growth phenotype of *big* alleles (Gil et al., 2001; Yamaguchi et al., 2007; 2013; Guo et al., 2013) and which has complex effects on suberin synthesis and degradation in the endodermis in Arabidopsis (Ursache et al., 2016; Cook et al., 2021). It is tempting to speculate that dysregulation of auxin synthesis and transport underpin the reduced suberization in *big-2*, however, there was no significant enrichment in transcripts related to auxin signalling pathways in *big-2* roots, in contrast to a previous transcriptome analysis employing leaves of a different *big* allele (Bruggeman et al., 2020). Whilst it is possible that there are tissue-specific

differences in auxin-related gene expression that are not detected in the bulk root transcriptome, other mechanisms regulating suberin in *big-2* roots cannot yet be ruled out.

Taken together, our study provides evidence that BIG not only participates in the N-degron pathways, impacting different aspects of plant physiology, but also influences other processes. This raises interesting mechanistic questions regarding the operation of BIG in N-degron and possibly other proteostatic pathways. BIG contains numerous protein-protein interaction domains (Supplementary Fig. 1; Gil et al., 2001) providing a platform for interaction with diverse protein partners and substrates. Proximity labelling identified both PRT6 and BIG as potential R-TurboID-interacting proteins (Fig. 2C), suggesting that BIG (like PRT6) may bind Arg/N-degrons, although a mutually compatible hypothesis is that BIG exists in a complex with PRT6 (see below). Reporter experiments revealed that BIG also works in concert with the PRT1 E3 ligase to mediate degradation of F-GUS (Fig. 1). Thus, BIG likely acts as an N-recognin for both type 1 and type 2 substrates. This is consistent with the domain structure of BIG. The mammalian N-recognins, UBR1 and 2 bind type 1 substrates via the UBR box and type 2 substrates at the Clp-S-like N-domain (Kim et al., 2021). BIG, UBR4 and PRT6 each contain UBR boxes but lack the N-domain (Tasaki et al., 2005; 2009; Garzón et al., 2007). Whereas the UBR box of PRT6 binds type 1 degrons, the UBR box of UBR4 recognises both type 1 and 2 N-termini through a distinct mechanism (Kim et al., 2020; 2021; 2022; Jeong et al., 2023). PRT1 also lacks a ClpS-like domain and may recognise type 2 substrates via a ZZ domain, which is also present in BIG (Stary et al. 2003).

An important question is whether BIG possesses intrinsic E3 ligase activity. Although BIG does not contain either a canonical E3 ligase Really Interesting New Gene (RING) or HECT domain, it shares with UBR4 a “hemiRING” zinc finger, which serves as an affinity factor for the recruitment of E2 ubiquitin conjugating enzymes (Barnsby-Greer et al., 2024), strongly suggesting that it also an E3. Notably, however, neither R-substrates nor F-substrates were stabilised in the single *big-2* mutant, suggesting that PRT6 and PRT1 are the dominant N-recognins *in planta*, with BIG providing a lower level of substrate turnover that is only detectable in the absence of PRT6 and PRT1. Ultimately, it will only be possible to test this in a

reconstituted system with purified PRT6/PRT1, BIG and the respective E2 and E1 enzymes, which would undoubtedly be extremely challenging. An alternative scenario is that BIG may play a more general role to prevent the release of potentially toxic, partly degraded proteins from the proteasome, recognising them via their neo-N-termini and a contribution to the turnover of N-degron pathway substrates is a consequence of this (Besche et al., 2009). BIG may also participate in autophagic pathways as is the case for UBR4 (Tasaki et al., 2013).

Given that UBR4 interacts with a diverse array of protein partners including E2 ubiquitin conjugating enzymes and E3 ligases to degrade both N-degron pathway substrates and other protein targets (Ashton-Beaucage et al., 2016; Yau et al., 2017; Hunt et al., 2019), it is plausible that BIG not only serves as a versatile recognition component of the Arg/N-degron pathways but also participates in other proteostatic mechanisms, interacting with one or more E3 ligases to mediate proteasomal degradation of a broad range of substrates (Fig. 7). Regulatory proteasome subunits and the HECT E3 ligases, ubiquitin protein ligase (UPL)1, UPL2 and UPL3 were enriched in R-TurboID samples (Fig. 2), which may indicate the presence of an N-recognin/E3 ligase complex at the proteasome. In agreement with this, BIG co-purified with proteasome subunits and UPL1/3 in transiently transfected *Nicotiana benthamiana* (Üstün et al., 2016). These observations are also consistent with previous reports of E3 ligases associated with the proteasome, including HECT E3 ligases (Wang and Spoel, 2022) and yeast Ubr1 (Xie and Varshavsky, 2000).

In yeast, the HECT E3 ligase Ufd4 binds Ubr1 and increases processivity of polyubiquitination (Hwang et al., 2010); similarly in plants, substrates from diverse E3 ligases are relayed to UPLs which prevent substrate stalling at the proteasome (Wang and Spoel, 2022). UBR4 is present at the proteasome at sub-stoichiometric amounts in mammals (Besche et al., 2009; 2014) and not only co-purifies with UPL-type HECT E3 ligases but also regulates the proteolytic activity of the proteasome (Hunt et al., 2019; Hunt et al., 2021). Collectively, this points to the existence of a proteostatic hub that is evolutionarily conserved but which has different interactors and substrates in plants and animals.

In conclusion, we have demonstrated that BIG participates in the Arg/N-degron pathways, contributing to the turnover of ERFVII transcription factors and VRN2 in

the context of oxygen signalling and have shown that this does not underpin all of the known growth phenotypes associated with loss of *BIG* function. Key challenges for future work will be to identify additional substrates and E3 ligases associated with BIG and link them to its physiological functions.

Materials and Methods

Plant material

All Arabidopsis (*Arabidopsis thaliana*) genetic material used in this study is listed in Supplementary Table 1. This study utilises *big-2* (SALK_045560) (Supplementary Fig. 1; Kasajima et al., 2007; Ivanova et al., 2014). N-degron pathway mutants *prt6-5, prt6-1,* and *ate1 ate2* were crossed to *big-2 to* generate the double mutants *prt6-5 big-2*, *prt6-1 big-2*, and *big-2 ate1 ate2* triple mutant. N-degron pathway mutant alleles expressing Pro35S:DHFR-Ub-X-GUS reporter lines (Garzón et al., 2007), ProUBQ3:X-LUC reporter lines (Worley et al., 1998; Graciet et al., 2010), and ProVRN2:VRN2:GUS (Gibbs et al., 2018) were crossed to *big-2* or *prt6-1 big-2* and Pro35S:HRE2-HA in Col-0 (Gibbs et al., 2011) was crossed to *prt6-5 big-2* and segregated into different backgrounds. Pro35S:RAP2.3-HA in Col-0 (Gibbs et al., 2014) was crossed to *big-2* and *prt6-5*, respectively, the resultant lines were crossed to each other, and seeds were maintained as Pro35S:RAP2.3-HA *prt6-5-/- big+/-.* Higher order loss of function mutants were obtained by crossing *rap2.12 rap2.2 rap2.3*, *prt6-1 rap2.12 rap2.2 rap2.3* (Gibbs et al., 2014), and *vrn2-5 prt6-1* (Gibbs et al., 2018), to *big-2* and *prt6-1 big-2*. Where N-degron pathway reporters were compared in different genetic backgrounds, all lines were generated by crossing of a specific transgenic line, such that all genotypes within a given experiment contain the same transgene event. All material was validated by PCR- or CAPS-based genotyping. Details of primers are given in Supplementary Data Set 3. The *big-2* mutant was re-sequenced (~25 x raw coverage) by the Earlham Institute, using Low Input, Transposase Enabled (LITE) library preparation and the Illumina NovaSeq 6000 S4 v1.5 platform. The positions of T-DNAs were identified by a BLAST search using the pBIN-pROK2 insertion sequences (http://signal.salk.edu/cgi-bin/tdnaexpress) as query.

Constructs for proximity labelling are based on vector R4 GWB601 (Mair et al., 2019), obtained from Addgene, and transformed into Col-0. The amino acid sequence for R-Turbo (2548_HpaI_Turbo-NESYFP) is shown in Supplementary Fig. 14, its M-Turbo counterpart differs by only two bases (exchange ATG for AGA, codon for first amino acid after ubiquitin cleavage).

R-LUC reporter lines in a wild-type Col-0 background (Graciet et al., 2010); based on constructs generated by (Worley et al., 1998) were crossed with *prt6-5*, *big-2* and *prt6-5 big-2* mutants. Lines containing the R-LUC reporter were selected on 0.5X MS + 0.5% (w/v) sucrose, 0.8 % (w/v) agar plates containing 20 mg/L Basta, and subsequently (i) genotyped to isolate homozygous mutants for *big-2* and *prt6-5*; and (ii) sequenced to confirm the identity of the R-LUC reporter.

Growth of Arabidopsis

Seeds were raised from plants grown in Levington's F2S compost under long day conditions (16 h day/8 h night; 23°C/18°C) light intensity of 250 µmol photons m^{-2} s^{-1} (Sunlight replica NS1, Valoya); all genotypes to be compared were raised in the same controlled environment cabinet. Seeds were harvested, sieved (< 425 µm; Endecotts, London, UK) and stored at room temperature. After-ripened seeds were surface-sterilised and sown on 0.5X Murashige and Skoog (MS) medium containing 0.5-1% (w/v) sucrose and 0.8% (w/v) plant agar (Duchefa). After 2-3 d dark chilling at 4°C, plates were grown in long day conditions (16 h/8 h; 22°C) for 4 to 10 d light intensity of 150 µmol photons m^{-2} s^{-1} (T5 54-watt fluorescents, Sylvania). .

Genotyping

For DNA isolation, frozen tissue samples [1-2 leaves from soil-grown plants or ~20 seedlings grown on 0.5X MS + 0.5% (w/v) sucrose and 0.8% (w/v) agar plates] were homogenised using a Geno/Grinder® (1750 rpm for 1.5 min) equipped with metal blocks pre-chilled with liquid N_2. 500 µL pre-warmed CTAB buffer [2% (w/v) cetyl trimethylammonium bromide, 1% (w/v) polyvinyl pyrrolidone (MW = 40,000), 1.4 M NaCl, 0.1 M Tris HCl, 20 mM EDTA, pH 5.0] was added to the powder, and incubated at 60°C for 30 min. Samples were centrifuged at 10,000 x g for 5 min, 5 µL RNase-A (10 mg/mL) was added to the supernatant and incubated for 15 min at room temperature. DNA was extracted by addition of an equal volume of

chloroform/isoamyl alcohol (24:1 v/v). Following centrifugation at 13,000 x g for 1 min, DNA in the upper aqueous phase was precipitated by adding 0.7 vol of isopropanol and incubating at -20°C for 15 min. DNA was pelleted by centrifugation at 13,000 x g for 10 min and the pellet washed twice with 400 µL pre-chilled 70% (v/v) ethanol and dried briefly, before dissolving in 100 µL TE buffer (10 mM Tris, 1 mM EDTA, pH 8.0). PCR was performed using a 20 µL total reaction volume, consisting of: 1X DreamTaq Green PCR Master Mix, 500 nM Forward Primer, 500 nM Reverse Primer, 10% (v/v) plant genomic DNA. Primers used are given in Supplementary Data Set 3.

GUS staining

Six d-old seedlings grown on 0.5X MS + 0.5% (w/v) sucrose and 0.8% (w/v) agar plates were immersed in 1 mL GUS assay buffer [100 mM sodium phosphate buffer (pH 7.0), 0.1 % (v/v) Triton X-100, 0.5 mg/mL X-GlucA, 500 µM potassium ferricyanide, 500 µM potassium ferrocyanide] in sterile 24-well plates, vacuum infiltrated for 30 min in darkness, then wrapped in foil and incubated at 37 °C overnight. Chlorophyll was removed by incubation in 85% (v/v) ethanol, 15% (v/v) acetic acid with gentle agitation for 2-4 h until cleared, after which the seedlings were placed in sterile water. In each independent experiment, at least 10 seedlings were stained per genotype and 4-5 representative seedlings were arranged onto agar plates for photography.

X-LUC assays

Seedlings stably expressing the R-LUC N-degron reporter construct were grown vertically on 0.5X MS + 0.5% (w/v) sucrose and 0.8% (w/v) agar plates containing 20 mg/L Basta to select for the presence of the reporter. Plates were kept at 4ºC in the dark for 3 days and then transferred to continuous light at 19.5°C for 7 days (~100 µmol m^{-2} s^{-1} bulbs used: Philips 6500K T8 14.5W). Forty seedlings per genotype and per biological replicate were harvested and immediately frozen in liquid nitrogen. Frozen tissue was ground using a drill and pestle and the powder was split equally between two tubes for (i) LUC enzymatic assays and (ii) RNA extraction followed by RT-qPCR to normalize the LUC enzymatic activities to the expression of the *LUC* gene in each of the samples. Four biological replicates per genotype, each

comprising 40 seedlings grown on separate plates were prepared and analyzed for both assays.

To test the enzymatic R-LUC activity, proteins were extracted from frozen ground tissue using 1x Luciferase Cell Culture Lysis Reagent (CCLR) (Promega), supplemented with 1 mM phenylmethylsulfonyl fluoride (PMSF) and 1:100 plant Protease Inhibitor Cocktail (Sigma-Aldrich). Samples were centrifuged at 12,000 x g for 10 minutes at 4°C to pellet cellular debris. Protein concentration was determined using the Bradford protein assay. Enzymatic LUC activity was measured as described in (Graciet et al., 2010; Luehrsen et al., 1992). Briefly, CCLR protein extract (1 µL) was added to 100 µL LAR buffer (20 mM tricine, pH 7.8, 1.07 mM $(MgCO_3)_4.Mg(OH)_2.5H_2O$, 2.67 mM $MgSO_4$, 0.1 mM ethylenediaminetetraacetic acid (EDTA), 33.3 mM dithiothreitol (DTT), 270 µM coenzyme A, 470 µM luciferin, 530 µM ATP) in a 96-well plate (Sterilin). Luminescence was measured using a POLARstar Omega microplate reader (BMG LABTECH) for 10 seconds.
To determine expression levels of the R-LUC reporter, total RNA was extracted using the Spectrum Plant Total RNA Kit (Sigma Aldrich/Merck) according to the manufacturer's instructions. Reverse transcription reactions were set up using 1000 ng of total RNA, RevertAid Reverse Transcriptase (Thermo Fisher) and associated buffer, RiboLock Rnase inhibitor (Thermo Fisher), oligo(dT)18 and 1 mM dNTP mixture at 42°C for 45 minutes. RT-qPCR reaction mixtures were prepared in LightCycler 480 96-well plates (Roche) with 1 µL of cDNA, 1 µL of primer pair mixture (1 µM final concentration each primer; Supplementary Data Set 3), 5 µL 2x SYBR green master mix (Roche), with nuclease-free water added to a final volume of 10 µL per well. RT-qPCR reactions were carried out in a LightCycler 480 instrument (Roche). The second derivative maximum method was used to determine crossing point (Cp) values.

Immunoblotting

Six-day-old roots or seedlings were harvested. Protein extraction and immunoblotting were performed as described in (Zhang et al., 2018a), with the exception that 1% (w/v) BSA in PBS-T was used as the blocking agent in the case of the anti-Biotin blots. Briefly, proteins were separated in precast 4–12% (w/v) Bis-Tris gels using 1X SDS MES buffer and transferred to polyvinylidene fluoride using

iBlot™ 2 Dry Blotting System (ThermoFisher, Waltham, MA, USA). Primary antibodies were used at the following dilutions: ADH (AS10685; Agrisera, Sweden), 1:3000; PGB1 (raised in rabbit to full-length recombinant protein; Hartman 2018) 1:3000, GUS (G5420; Sigma-Aldrich), 1:1000; HA (H 3663; Sigma) 1:1000, and biotin (BN-34; Sigma) 1:2,000. The secondary antibodies used were anti-rabbit horseradish peroxidase conjugate (A0545; Sigma) diluted 1:50,000 (for ADH, PGB1 and GUS), m-IgGk BP-HRP (sc-516102; Santa Cruz Biotechnology) diluted 1:15,000 (for HA) or anti-mouse IgG-HRP (NA931; GE Healthcare) diluted 1:10,000 (for biotin). Blots were then washed and developed with SuperSignal™ West Pico PLUS Chemiluminescent Substrate (Thermo Fisher Scientific).

Reverse transcription quantitative PCR (RT-qPCR)

Six-day-old roots or seedlings were harvested, frozen in liquid nitrogen, and homogenized using the Geno/Grinder® as described for "Genotyping". Total RNA was extracted using an RNeasy Plant Mini Kit (Qiagen) and treated using a TURBO DNA-free™ Kit (Invitrogen™), or a Monarch® Total RNA Miniprep Kit (New England Biolabs, Inc), with on-column DNAse I treatment. A RevertAid™ First Strand cDNA Synthesis Kit (Thermo Scientific) and anchored -oligo(dT)18 were used for cDNA synthesis for a two-step RT-PCR. SYBR® Green JumpStart™ Taq ReadyMix™ was used for real-time PCR using a Lightcycler® 96 Instrument (Roche) or a Quantstudio 6 Pro (Thermo), according to manufacturers' instructions. Three to four biological replicates, each consisting of 20 seedlings or 100 primary roots grown on separate plates, were included for each genotype. Two technical replicates were prepared per cDNA sample and primer combination. Relative quantification was performed using both *ACTIN 2* (*ACT2;* At3g18780.2) and *TUBULIN BETA CHAIN 4* (*TUB4*; At5g44340.1) as references. For the experiments presented in Fig. 4C, 4E and Supplementary Fig. 8, a single reference gene (*ACT2*) was used due to practical constraints. *POLYUBIQUITIN10* (*UBQ10*; At4g05320.2) and At5g18800 were used as references for the experiments presented in Fig. 6B and Supplementary Fig. 13B. Relative gene expression was calculated using the $2^{-\Delta\Delta Ct}$ method (Livak and Schmittgen, 2001), using the threshold cycles automatically determined by the software to obtain fold-change values, which were then normalized to the mean fold-change of Col-0. Data were natural log transformed for statistical analysis and

visualization when indicated, as appropriate by linear modelling. Primers used are given in Supplementary Data Set 3.

Hypoxia and waterlogging assays

Hypoxic conditions were imposed by anaero atmosphere generation bags (68061 Sigma) in an anaerobic jar (28029 Sigma) according to the manufacturer's instructions. Seedlings were grown on 0.5X MS + 0.5% (w/v) sucrose plus 0.8% (w/v) plant agar, and treated with hypoxia in the dark by enclosing the plates in an anaerobic jar, from which oxygen was reduced to below 1% within 1 h, monitored by smart sensor Oxygen Detector AR8100. Controls were kept in the dark for the same period of time under normal oxygen conditions. For chlorophyll measurement, 4-d old seedlings were treated for 5 h, then returned to the light for 3 d recovery, seedlings were photographed, weighed, and submerged in 80% (v/v) acetone overnight at 4°C, in darkness. Absorbance at 646 nm and 663 nm was used to estimate total chlorophyll (Lichtenthaler et al., 1983). For survival scoring, seedlings were assigned a score based on their appearance as in (Gibbs et al., 2011): 1 for no remaining chlorophyll, 3 for partial chlorophyll coverage, and 5 for complete chlorophyll coverage. Scores were aggregated to produce a mean survival score for each plate containing 20–30 seedlings. For the root regrowth assay, 7 seeds per genotype were sown on the same plates; four different configurations of plates were prepared, varying which position each genotype occupied, with 3 replicates per configuration. Therefore, there were 12 plates considered as biological replicates per treatment. Five-d old seedlings were treated for 4 h, then the plates were turned 90 degrees and photographed after 2 d recovery in the light. Regrowth, as indicated by bending of the primary roots was scored. Waterlogging tolerance was assayed as described in Gibbs et al., (2018).

Suberin quantification

Seeds were surface-sterilised and plated on 0.5X MS + 0.5% (w/v) sucrose containing 0.8 % (w/v) agar. After 2–3 d dark chilling at 4°C, seedlings were grown vertically in long days (16 h/8 h; 22°C) for 5 days and stained with Fluorol Yellow 088, as described in (Barberon et al., 2016). Tiled images were captured across whole seedlings using a Zeiss Axio Imager.Z2 microscope (10X objective and GFP fluorescence filters: excitation 450 – 490 nm; emission 500 – 550 nm, illumination

450 – 488 nm) and Zen3.0 blue edition software. Seedlings were initially viewed using brightfield imaging at a low light level to define the region to be scanned and create focal points (“support points”) along the length of the root. Entire seedlings were then scanned using fluorescence contrast imaging with 100% light intensity (excitation 488 nm; emission 509 nm) and a 10% overlap of tile images for alignment and stitching. Images were pseudo-coloured using the “YellowToWhite” LUT, annotated with a 1000 µm scale bar, and exported as TIFF files at 70% of the original size. Suberization patterns were quantified using ImageJ to measure the length of the different regions in µm: “suberized” for continuous suberization, “patchy” for partial suberization, and “non-suberized” for the region with no suberized cells. Results were expressed as the percentage of the total root length.

Cuticle staining

Cuticular integrity was assessed by Toluidine Blue staining, according to Tanaka et al., 2004. Briefly, 8 d old seedlings grown on 0.5X MS + 1 % (w/v) sucrose + 0.8 % (w/v) agar plates were immersed in an aqueous solution of 0.05 % (w/v) Toluidine Blue O (Sigma-Aldrich, St Louis, MO, USA) for 2 min, rinsed twice with water, and arranged onto agar plates for photography.

Statistical analysis

Statistical analyses were performed on comparable sets of data using the R environment and are presented in Supplementary Data Set S4. For analysis of multiple genotypes, transgenic lines, and/or treatments, base R was used to perform ANOVA, and the R packages “emmeans”, “predictmeans”, and “multcomp” were used for subsequent Tukey multiple comparisons tests. All packages are available from CRAN (https://cran.r-project.org/). Prior to statistical testing, data were log transformed if indicated as necessary by linear model fitting. All statistical tests performed were two-sided.

Bar plots presented in this paper display mean values with individual data points overlaid, and error bars indicate standard deviation. Unique letters indicate statistically significant differences between groups ($P<0.05$). Box plots display the median as the centre line, the upper and lower quartiles as the box limits, 1.5x the interquartile range as whiskers, and individual data points are overlaid.

RNA-seq

After-ripened seeds were surface-sterilised and plated on nylon mesh (Sefar NITEX, 03-110/47; Heiden, Switzerland) overlaid on 0.5X Murashige and Skoog (MS) medium containing 0.5 % (w/v) sucrose and 0.8% (w/v) plant agar in square plates (688161, Greiner). One cm sections containing the root tip were harvested from 5-d old seedlings, frozen in liquid nitrogen, and RNA was extracted using an RNeasy Plant Mini Kit (Qiagen) and treated using a TURBO DNA-free™ Kit (Invitrogen™). Five biological replicates per genotype were prepared; an individual plate comprised a biological replicate. RNA sequencing and data analysis were done using Illumina HiSeq (2 x 150 paired end reads) by Genewiz. Briefly, sequence reads were trimmed to remove possible adapter sequences and nucleotides with poor quality using Trimmomatic v.0.36. The trimmed reads were mapped to the *Arabidopsis thaliana* TAIR10 reference genome available on ENSEMBL using the STAR aligner v.2.5.2b. Unique gene hit counts were calculated by using feature Counts from the Subread package v.1.5.2. Only unique reads that fell within exon regions were counted. Since a strand-specific library preparation was performed, the reads were strand-specifically counted. Differential expression analysis was performed using DESeq2. The Wald test was used to generate p-values and log2 fold changes. Genes with an adjusted p-value < 0.05 and absolute log2 fold change > 1 were called as differentially expressed genes for each comparison.

Proximity labelling

Arabidopsis plants (15 seedlings per well, 24 well plate) were grown in liquid culture [1mL 1x MS medium with 1% (w/v) sucrose per well] for 1 week under long day conditions (23°C, 16 h light from cool white fluorescent bulbs). Medium was exchanged with medium supplemented with 10 µM Bortezomib and 50 µM biotin 75 min before harvest. Plants were washed 4x with 2 mL ice cold water, then 1 mL ice cold water was added before they were dried and snap frozen in liquid N_2. Tissue was homogenised in a pre-cooled Tissue Lyser (2x 10 min, 28 Hz) and 170 µL extraction buffer [50 mM Tris pH 7.5; 150 mM NaCl; 1 mM EDTA; 0.5% (v/v) NP-40 substitute; 3 mM DTT; plant protease inhibitor cocktail (Sigma)] added. Extracts from 3 wells were pooled (= ~500 µl crude extract as input). After centrifugation at 4°C, 500 µL of the supernatant was loaded onto a Sephadex G-25 column (Cytiva

MiniTrap PD-10) and eluted with 1 mL extraction buffer to remove free biotin. The protein concentration of the eluate was determined by Bradford assay and amounts of extracts were adjusted to the sample with the lowest protein concentration (2.3 mg total protein). Samples were incubated with Pierce Magnetic Streptavidin beads equilibrated in extraction buffer (25 µL beads per sample) for 60 min with rotation at 4°C. The beads were washed 4x with 1 mL wash buffer (20 mM Tris pH 7.5; 500 mM NaCl; 0.5 mM EDTA), transferred to a fresh low binding tube, washed again with 1 mL wash buffer and finally resuspended in 500 µL wash buffer. Three technical replicates per genotype were submitted to proteomic analysis. Two additional biological replicates (each including technical replicates) gave similar results.

Sample preparation for mass spectrometry analysis

The beads from the proximity labelling reactions were resuspended in 50 µL 1 M urea, 50 mM ammonium bicarbonate. Disulfide bonds were reduced with 2 µL of 250 mM dithiothreitol (DTT) for 30 min at room temperature before adding 2 µL of 500 mM iodoacetamide and incubating for 30 min at room temperature in the dark. The remaining iodoacetamide was quenched with 1 µL of 250 mM DTT for 10 min. Proteins were digested with 150 ng LysC (mass spectrometry grade, FUJIFILM Wako chemicals) in 1.5 µL 50 mM ammonium bicarbonate at 25°C overnight. The supernatant without beads was digested with 150 ng trypsin (Trypsin Gold, Promega) in 1.5 µL 50 mM ammonium bicarbonate followed by incubation at 37°C for 5 hours. The digest was stopped by the addition of trifluoroacetic acid (TFA) to a final concentration of 0.5 % (w/v), and the peptides were desalted using C18 Stagetips (Rappsilber et al., 2007).

Liquid chromatography-mass spectrometry analysis

Peptides were separated on an Ultimate 3000 RSLC nano-flow chromatography system (Thermo Fisher), using a pre-column for sample loading (Acclaim PepMap C18, 2 cm × 0.1 mm, 5 µm, Thermo Fisher), and a C18 analytical column (Acclaim PepMap C18, 50 cm × 0.75 mm, 2 µm, Thermo Fisher), applying a segmented linear gradient from 2% to 35% and finally 80% (v/v) solvent B [80 % (v/v) acetonitrile, 0.1 % (v/v) formic acid; solvent A 0.1 % (v/v) formic acid] at a flow rate of 230 nL/min over 120 min.

Eluting peptides were analysed on an Exploris 480 Orbitrap mass spectrometer (Thermo Fisher) coupled to the column with a FAIMS pro ion-source (Thermo Fisher) using coated emitter tips (PepSep, MSWil) with the following settings: the mass spectrometer was operated in DDA mode with two FAIMS compensation voltages (CV) set to -45 or -60 and 1.5 s cycle time per CV. The survey scans were obtained in a mass range of 350-1500 m/z, at a resolution of 60k at 200 m/z, and a normalized AGC target at 100%. The most intense ions were selected with an isolation width of 1.2 m/z, fragmented in the HCD cell at 28% collision energy, and the spectra recorded for maximum 100 ms at a normalized AGC target of 100% and a resolution of 15k. Peptides with a charge of +2 to +6 were included for fragmentation, the peptide match feature was set to preferred, the exclude isotope feature was enabled, and selected precursors were dynamically excluded from repeated sampling for 45 s.

Proteomics data analysis

MS raw data split for each CV using FreeStyle 1.7 (Thermo Fisher), were analysed using the MaxQuant software package (version 2.1.0.0; Tyanova et al., 2016) with the Uniprot *Arabidopsis thaliana* reference proteome (version 2022.01 www.uniprot.org), target sequences, as well as a database of the most common contaminants. The search was performed with full trypsin specificity and a maximum of two missed cleavages at a protein and peptide spectrum match false discovery rate of 1%. Carbamidomethylation of cysteine residues was set as fixed, oxidation of methionine, and N-terminal acetylation as variable modifications. For label-free quantification the “match between runs” only within the sample batch and the LFQ function were activated - all other parameters were left at default. MaxQuant output tables were further processed in R 4.2.1 (https://www.R-project.org) using Cassiopeia_LFQ (https://github.com/moritzmadern/Cassiopeia_LFQ). Reverse database identifications, contaminant proteins, protein groups identified only by a modified peptide, protein groups with less than two quantitative values in one experimental group, and protein groups with less than 2 razor peptides were removed for further analysis. Missing values were replaced by randomly drawing data points from a normal distribution model on the whole dataset (data mean shifted by -1.8 standard deviations, a width of the distribution of 0.3 standard deviations).

Differences between groups were statistically evaluated using the LIMMA 3.52.1 (Ritchie et al., 2015) at 5% FDR (Benjamini-Hochberg

Accession numbers

Sequence data from this article can be found in the EMBL/GenBank data libraries under accession numbers:

AT3G24800, AT5G02310, AT3G02260, AT5G05700, AT3G11240, AT1G53910, AT3G14230, AT3G16770, AT2G47520, AT4G16845, AT1G55860, AT1G70320, AT4G38600, AT5G39890, AT5G15120, AT4G33070, AT4G27450, AT4G24110, AT4G10270, AT3G23150, AT3G02550, AT3G10040, AT1G19530, AT1G43800, AT1G33055, AT2G16060, AT2G17850, AT1G77120, AT2G19590, AT4G17670, AT1G35140, AT1G26270, AT5G26200, AT5G66985, AT5G62520, AT5G61440, AT5G58070, AT5G54960, AT5G47910, AT5G47060, AT5G45340, AT5G44730, AT5G42200, AT5G10040, AT5G02200, AT3G61060, AT3G43190, AT4G39675, AT4G33560, AT4G32840, AT4G22780, AT3G27220, AT3G23170, AT3G17860, AT1G63090, AT1G76650, AT1G17290, AT1G74940, AT1G72940, AT1G55810, AT2G34390, AT1G51680, AT1G65060, AT2G39350, AT1G17840, AT2G37360, AT3G53510, AT5G13580, AT5G41040, At2g40890, AT2G30490, AT1G67990, AT4G34050, AT4G26220, AT5G58860, AT5G23190, AT5G08250, AT5G63450, AT3G48520, AT5G63560, AT5G22500, AT3G44540, AT3G44550, AT1G28650, AT1G54000, AT1G74460, AT2G19050, AT2G23540, AT2G30310, AT3G48460, AT3G50400, AT4G26790, AT5G37690, AT3G11430, AT5G06090, AT1G01120, AT4G34510, AT1G04220, AT5G43760, AT1G68530, AT1G49430, AT2G38530, AT2G48130, AT1G55260, AT2G37040, AT3G53260, AT5G04230, AT3G10340, AT3G61680.

Genome re-sequencing data are deposited in the NCBI Sequence Read Archive, accession number PRJNA1046295. The RNA-seq data files for this study have been uploaded to NCBI (https://www.ncbi.nlm.nih.gov/) under project number PRJNA975350, with accession numbers SAMN35345055-SAMN35345074. The mass spectrometry proteomics data have been deposited to the ProteomeXchange Consortium via the PRIDE (Perez-Riverol et al., 2022) partner repository with the dataset identifier PXD041610.

Supplementary Data

Supplementary Figure S1. Details of the *big-2* allele.

Supplementary Figure S2. BIG influences the stability of a model type 1 Arg/N-degron pathway substrate.

Supplementary Figure S3. Morphology of seedlings ectopically expressing RAP2.3-HA.

Supplementary Figure S4. Morphology of plants ectopically expressing RAP2.3-HA.

Supplementary Figure S5. Morphology of PRT6/N-degron pathway and *erfvii* combination mutants.

Supplementary Figure S6. Hypoxia response of PRT6/N-degron pathway mutants.

Supplementary Figure S7. Response of PRT6/N-degron pathway mutants to hypoxia and waterlogging.

Supplementary Figure S8. Relative expression of hypoxia-responsive genes in N-degron pathway mutants.

Supplementary Figure S9. Transcriptome analysis of N-degron pathway mutants.

Supplementary Figure S10. Gene Ontology term enrichment in genes up-regulated in roots of N-degron pathway mutants.

Supplementary Figure S11. Gene Ontology term enrichment in genes down-regulated in roots of N-degron pathway mutants.

Supplementary Figure S12. Suberin biosynthesis and deposition in N-degron pathway mutants.

Supplementary Figure S13. Relative expression of hypoxia and suberin biosynthesis and deposition genes in *big-2* combination mutants lacking the *plip1-3* T-DNA.

Supplementary Figure S14. Amino acid sequence of R-Turbo and M-Turbo.

Supplementary Table S1. Genetic materials used in this study.

Supplementary Data Set S1. TurboID proteomics data.

Supplementary Data Set S2. RNA-seq data.

Supplementary Data Set S3. Primers used in this study.

Supplementary Data Set S4. Details of statistical analysis.

Funding information

Work at Rothamsted Research was funded by the Biotechnology and Biological Sciences Research Council (BBSRC) through the Tailoring Plant Metabolism for the Bioeconomy Institute Strategic Grant BBS/E/C/000I0420 and the Green Engineering Institute Strategic Grant BB/X010988/1. Work in A.B.´s lab was supported by grant F7904B from the Austrian Research Agency FWF. Work in E.G.'s lab was supported by grant 13/IA/1870 from Science Foundation Ireland and by an Irish Research Council PhD scholarship (GOIPG/2017/2) to B.C.M.

Acknowledgments

We thank Daniel Gibbs and Michael Holdsworth for sharing genetic materials, Kirsty Hassall for statistical advice, David Hughes and Steve Hanley for help with bioinformatics, Lucy Gannon for assistance with initial genetic crosses, and Graham Shephard for photography. We are indebted to Xiaowei Li for help exporting statistical reports. Re-sequencing the *big-2* allele was carried out by the Earlham Institute. Proteomics analyses were performed by the Mass Spectrometry Facility at Max Perutz Labs using the VBCF instrument pool. The authors would like to thank the anonymous reviewers for constructive suggestions that contributed to improving the revised manuscript.

Author Contributions

The work was conceived by FLT and HZ. HZ and CR generated and characterised the genetic materials and conducted RT-qPCR, immunoblot, histochemical, physiological and transcriptome analysis. NW and AB performed the proximity labelling study; BCM, AM, and EG contributed the X-LUC data and generated *ate1/2 big-2*. All authors analysed data. FLT wrote the paper which was reviewed and edited by all authors before submission.

Figure 1. BIG influences the stability of model type 1 and type 2 Arg/N-degron pathway substrates.

(A) Schematic showing the architecture of the Arg/N-degron pathway and specificity of N-recognins in plants and mammals. Single letter codes for amino acid residues are used; *C indicates oxidised cysteine. Proteins (represented by grey ovals) may

become N-degron pathway substrates via cleavage by non-processive endopeptidases (EP), or by methionine aminopeptidase (MetAP), where the second residue is small. Substrates may also be generated by enzymatic modification of N-termini by PLANT CYSTEINE OXIDASE (PCO), Asn-specific N-terminal amidase (NTAN), Gln-specific N-terminal amidase (NTAQ), and arginyl-tRNA protein transferase (ATE). In plants, destabilising residues thus generated are targeted for degradation by the Ubiquitin Proteasome System (UPS) via N-recognin E3 ligases PROTEOLYSIS6 (PRT6; specific for basic N-termini) and PROTEOLYSIS1 (PRT1; specific for aromatic N-termini). In mammals, four N-recognins act semi-redundantly to mediate the degradation of both type 1 and type 2 substrates via the UPS or by autophagy. (B) Generation of N-degron pathway X-GUS substrates. Constructs driven by the constitutive *CaMV35S* promoter (Pro35S) encode a fusion of mouse dihydrofolate reductase (DHFR, yellow) to ubiquitin (variant K48R; Ub, white), followed by *Escherichia coli* beta glucuronidase (GUS, blue). Ubiquitin-specific proteases (indicated by the scissors icon) remove ubiquitin co-translationally to release the GUS reporter protein and reveal a new N terminus (residue of choice, X). The GUS ORF is extended by unstructured amino acids (black) to enhance the effect of destabilising amino-terminal residues. The cleavage also creates a stable DHFR reference protein and HA epitopes enable immunological detection of both products (Garzón et al., 2007). NOS, nopaline synthase terminator. Note that the stable reference carries one copy of the HA epitope, whereas the reporter has three copies. (C-F) Detection of N-degron pathway substrates by immunoblotting of crude protein extracts from 6-d old seedlings of different genotypes expressing X-GUS reporters. Symbols to the left indicate the protein products shown in (B). Blots were developed until the stable reference protein could be detected (α-HA long); where the stabilised reporter band signal is saturated, a shorter exposure is shown in the lower panel (short) for clarity. Ponceau S staining was used to confirm equal loading. (G) Histochemical staining of GUS reporter activity in 6-d old seedlings expressing R-GUS and F-GUS test substrates. Representative seedlings were rearranged on an agar plate, prior to photography. Bar, 1 cm (images are scaled identically).

Figure 2. Identification of N-degron proximal proteins

(A) Schematic of construct used for proximity labelling assay. Turbo-NES-eYFP (Mair et al., 2019) was modified to harbour an N-terminal ubiquitin (Ub) fusion construct, comprising dihydrofolate reductase-HA epitope-Ub (DHFR-HA-Ub) followed by the N-terminal amino acid of choice (X) in front of a fusion comprising a linker sequence (black), the V5 epitope, modified *Escherichia coli* biotin ligase (Turbo), a nuclear export signal (NES) and enhanced yellow fluorescent protein (eYFP). The construct was expressed from the *POLYUBIQUITIN10* promoter (ProUBQ10). The fusion protein is cleaved in planta by ubiquitin specific proteases, indicated by the scissors icon. (B) Anti-biotin immunoblots to follow the enrichment of biotinylated protein in extracts from 7-d old Col-0 and plants expressing R-Turbo and M-Turbo. Lane 1, crude extract; lane 2, extract after desalting; lanes 3 and 4, supernatant after two subsequent incubations with streptavidin beads (unbound fractions); lane 5, streptavidin beads after first incubation. Black arrows indicate the bait proteins R-Turbo and M-Turbo (70.2 kDa), and the red arrow indicates a non-specific background band. (C) Volcano plot visualising enrichment of biotinylated proteins when comparing transgenic lines expressing R-Turbo versus M-Turbo, after proteasome inhibition to ensure equal presence of either protein. PRT6 and BIG (magenta squares) are the two most enriched proteins. Olive diamonds, non-ATPase subunits of the proteasome; blue circles, ATPase subunits; brown triangles, Homologous to the E6-AP Carboxyl Terminus (HECT) E3 ubiquitin ligases.

Figure 3. BIG influences the abundance of physiological PRT6/N-degron pathway substrates.

(A-C) Molecular analysis of seedlings expressing Pro35S:HRE2-HA. (A) Immunoblots of crude protein extracts from 6-d old roots of the indicated genotypes, probed with anti-HA (α-HA) antiserum or antibodies specific for the hypoxia markers, alcohol dehydrogenase (ADH) and phytoglobin1 (PGB1; the hypoxia marker antibodies were applied simultaneously to a single membrane). Ponceau S staining was used to confirm equal loading. (B) Expression of *HRE2* transgene relative to Col-0. Values are means ± SD (n=4). (C) Expression of *ADH* and *PGB1* relative to Col-0. Values are means ± SD (n=4). (D-G) Molecular analysis of seedlings expressing Pro35S:RAP2.3-HA. (D, G) Immunoblots of crude protein extracts from 6-d old seedlings of the indicated genotypes, probed with anti-HA (α-HA) antiserum

or antibodies specific for the hypoxia markers, ADH and PGB1. (E) Expression of *RAP2.3* transgene relative to Col-0. Values are means ± SD (n=4). (F) Expression of *ADH* and *PGB1* relative to Col-0. Values are means ± SD (n=4). (H-J) Molecular analysis of seedlings expressing ProVRN2:VRN2-GUS. (H) Histochemical staining of glucuronidase (GUS) reporter activity in 6-d old seedlings. Seedlings were rearranged on an agar plate prior to photography. Bar, 1 cm. (I) Immunoblot of 6-d old seedlings probed with anti-GUS antibody. (J) Expression of *VRN2* and *GUS* relative to Col-0. Values are means ± SD (n=4). For all plots, different letters indicate significant differences between conditions ($P < 0.05$; ANOVA with Tukey multiple comparison test).

Figure 4. Regulation of the hypoxia response by BIG requires ATE1/2 and ERFVIIs

(A,B) Molecular analysis of PRT6/N-degron pathway mutants. (A) Expression of *ADH* and *PGB1* relative to Col-0 in 6-d old seedlings. Values are means ± SD (n=4). (B) Immunoblots of crude protein extracts from 6-d old seedlings of the indicated genotypes, probed with antibodies specific for the hypoxia markers, alcohol dehydrogenase (ADH) and phytoglobin1 (PGB1) (which were applied to the same membrane). (C-F) Molecular analysis of PRT6/N-degron pathway mutants combined with *rap2.12 rap2.2 rap2.3* mutant alleles ("*rap triple*") (C,D) or with *vrn2-5* (E,F). (C,E) Expression of *ADH* and *PGB1* relative to Col-0 in 6-d old seedlings. Values are means ± SD (n=3). (D,F) Immunoblot of crude protein extracts from 6-d old seedlings of the indicated genotypes, probed with anti-HA (α-HA) antiserum or antibodies specific for the hypoxia markers, ADH and PGB1. Ponceau S staining was used to confirm equal loading. For all plots, different letters indicate significant differences between conditions ($P < 0.05$; ANOVA with Tukey multiple comparison test).

Figure 5. Impact of BIG on the root transcriptome

(A) Numbers of differentially expressed genes (DEGs) in roots of different mutant backgrounds. DEGs are defined as having a fold change greater than or equal to two at adjusted p-value<0.01. (B) Plots comparing the fold-change of transcripts in *big-2* and *prt6-5* single mutants with the double mutant, *prt6-5 big-2*. The dashed red line

indicates equal fold change in the two genotypes. (C) Venn diagram showing overlap of DEGs with hypoxia responsive genes in Arabidopsis roots (differentially regulated following 7h of dark submergence; Lee et al., 2011), indicated in red. (D) Heatmap showing log2 fold change of 49 “core hypoxia” genes (Mustroph et al., 2009) in the different mutant backgrounds relative to Col-0. Red and blue indicate up and down regulated genes, respectively. Gene names or AGI codes are shown to the left of the panel. (E) Scheme summarising impact of BIG on the N-degron pathway and the hypoxia response. Under normoxia, ERVII transcription factors and VRN2 are sequentially modified by methionine aminopeptidases (MetAP), plant cysteine oxidases (PCO) and arginyl-tRNA protein transferases (ATE1/2), such that the Nt Met is removed to reveal Cys2, which is oxidised (*C) and then arginylated (R*C). R*C-ERF and R*C-VRN2 are then targeted for degradation by PRT6 and also by a process involving BIG. Degradation is prevented in hypoxic conditions and in the absence of PRT6 (and BIG) function. The accumulation of ERFVIIs initiates the transcription of hypoxia responsive genes. The accumulation of VRN2 negatively influences the expression of certain hypoxia responsive genes.

Figure 6. PRT6 and BIG regulate suberin deposition in roots

(A) Heatmap derived from RNA-seq data showing log2 fold change of genes associated with suberin biosynthesis and deposition in the different mutant backgrounds, relative to Col-0. The gene list was curated from (Mustroph and Bailey-Serres, 2010; Ursache et al., 2021; Serra and Geldner, 2022). Gene names or AGI codes are shown to the left of the panel. (B) RT-qPCR analysis of genes involved in suberin biosynthesis and deposition in 5-d old roots of mutants, showing natural log of expression relative to Col-0. Values are means ± SD (n=4); different letters indicate significant differences between genotypes ($P < 0.05$). (C) Representative composite micrographs showing Fluorol Yellow 088 staining of suberin in wild type and mutant roots (scale bar represents 1 mm; images are scaled identically). The full root images are shown in Fig. S8. (D) Quantification of suberin deposition along the root axis using three different zones: non-suberized, patchy, and continuous. Data are presented as mean percentage coverage of root length ± SD (n=10 roots; representative of two independent experiments); different letters indicate significant

differences between genotypes for each region ($P < 0.05$; ANOVA with Tukey multiple comparison test).

Figure 7. Speculative model for action of PRT6 and BIG

The cartoon is based on information from the literature and data from the current study. A subset of the cellular pool of BIG and PRT6 is bound to the proteasome lid where the two proteins may interact (Xie & Varshavsky, 2000; Besche et al., 2009; 2014; Űstün et al., 2016; Fig. 2), but BIG and PRT6 likely also work without association with the proteasome, as indicated by the dashed lines around the proteasome and associated proteins. PRT6 is a candidate E3 ligase that works together with the E2 conjugating enzyme, UBC2 to ubiquitinate protein substrates with basic (type 1) N-termini, targeting them for proteasomal degradation (Garzón et al., 2007; Kozlic et al., 2022). BIG acts as a scaffold, recruiting one or more as-yet unidentified E3 enzymes (indicated by different colours) as well as E2 enzymes to ubiquitinate protein substrates with type 1 and type 2 N-termini, resulting in their degradation (Ashton-Beaucage et al., 2016; Yau et al., 2017; Hunt et al., 2019); Fig. 1E, F). Alternatively, BIG may have intrinsic E3 ligase activity, by analogy with UBR4 (Barnsby-Greer et al., 2024). The PRT1 E3 ligase also mediates degradation of aromatic (type 2) substrates, together with UBC8 (Stary et al., 2003; Mot et al., 2018). Several reports indicate that the HECT-type ubiquitin protein ligases (UPLs) reside at the proteasome, where they increase the processivity of polyubiquitination in concert with multiple E3 ligases (Hwang et al., 2010; Wang and Spoel, 2022).

References

Abbas M, Berckhan S, Rooney DJ, Gibbs DJ, Vicente Conde J, Sousa Correia C, Bassel GW, Marín-de la Rosa N, León J, Alabadí D, et al. (2015) Oxygen sensing coordinates photomorphogenesis to facilitate seedling survival. Curr. Biol. 25: 1483-1488

Abbas M, Sharma G, Dambire C, Marquez J, Alonso-Blanco C, Proaño K, Holdsworth MJ. (2022) An oxygen-sensing mechanism for angiosperm adaptation to altitude. Nature 606: 565-569

Ashton-Beaucage D, Lemieux C, Udell CM, Sahmi M, Rochette S, Therrien M. (2016) The Deubiquitinase USP47 Stabilizes MAPK by Counteracting the Function of the N-end Rule ligase POE/UBR4 in Drosophila. PLoS Biol. 14(8):e1002539

Bachmair A, Finley D, Varshavsky A. (1986) In vivo half-life of a protein is a function of its amino-terminal residue. Science 234: 179-186

Barberon M, Vermeer JE, De Bellis D, Wang P, Naseer S, Andersen TG, Humbel BM, Nawrath CJ, Takano J, Salt DE, et al. (2016) Adaptation of Root Function by Nutrient-Induced Plasticity of Endodermal Differentiation. Cell 164: 447-459

Barnsby-Greer L, Mabbitt PD, Dery MA, Squair DR, Wood NT, Lamoliatte F, Lange SM, Virdee S. (2024) UBE2A and UBE2B are recruited by an atypical E3 ligase module in UBR4. Nat Struct Mol Biol. doi: 10.1038/s41594-023-01192-4.

Besche HC, Haas W, Gygim SP, Goldberg AL. (2009) Isolation of mammalian 26S proteasomes and p97/VCP complexes using the ubiquitin-like domain from HHR23b reveals novel proteasome-associated proteins. Biochemistry 48: 2538-2549

Besche HC, Sha Z, Kukushkin NV, Peth A, Hock EM, Kim W, Gygi S, Gutierrez JA, Liao H, Dick L, et al. (2014) Autoubiquitination of the 26S proteasome on Rpn13 regulates breakdown of ubiquitin conjugates. EMBO J. 33: 1159-1176

Bruggeman Q, Piron-Prunier F, Tellier F, Faure JD, Latrasse D, Manza-Mianza D, Mazubert C, Citerne S, Boutet-Mercey S, Lugan R, et al. (2020) Involvement of Arabidopsis BIG protein in cell death mediated by Myo-inositol homeostasis. Sci. Rep. 10: 11268

Choy MK, Sullivan JA, Theobald JC, Davies WJ, Gray JC. (2008) An Arabidopsis mutant able to green after extended dark periods shows decreased transcripts of seed protein genes and altered sensitivity to abscisic acid. J. Exp. Bot. 59(14): 3869-3884

Ciechanover A. (2013).Intracellular protein degradation: from a vague idea through the lysosome and the ubiquitin-proteasome system and onto human diseases and drug targeting. Bioorg. Med. Chem. 21: 3400-3410

Cominelli E, Sala T, Calvi D, Gusmaroli G, Tonelli C. (2008) Over-expression of the Arabidopsis *AtMYB41* gene alters cell expansion and leaf surface permeability. Plant J. 53: 53-64

Cook SD, Kimura S, Wu Q, Franke RB, Kamiya T, Kasahara H. (2021) Regulation of suberin biosynthesis and Casparian strip development in the root endodermis by two plant auxins. BioRxiv doi:10.1101/2021.06.02.446769

de Marchi R, Sorel M, Mooney B, Fudal I, Goslin K, Kwaśniewska K, Ryan PT, Pfalz M, Kroymann J, Pollmann S, et al. (2016) The N-end rule pathway regulates pathogen responses in plants. Sci. Rep. 6: 26020

Desgagné-Penix I, Eakanunkul S, Coles JP, Phillips AL, Hedden P, Sponsel VM, (2005) The auxin *transport inhibitor response 3* (*tir3*) allele of *BIG* and auxin transport inhibitors affect the gibberellin status of Arabidopsis. Plant J. 41: 231-242

Dong H, Dumenil J, Lu FH, Na L, Vanhaeren H, Naumann C, Klecker M, Prior R, Smith C, McKenzie N, et al. (2017) Ubiquitylation activates a peptidase that promotes cleavage and destabilization of its activating E3 ligases and diverse growth regulatory proteins to limit cell proliferation in Arabidopsis. Genes Dev. 31: 197-208

Ejiri M, Fukao T, Miyashita T, Shiono K. (2021) A barrier to radial oxygen loss helps the root system cope with waterlogging-induced hypoxia. Breed Sci. 71: 40-50

Garzón M, Eifler K, Faust A, Scheel H, Hofmann K, Koncz C, Yephremov A, Bachmair A. (2007) PRT6/At5g02310 encodes an Arabidopsis ubiquitin ligase of the N-end rule pathway with arginine specificity and is not the *CER3* locus. FEBS Lett. 581: 3189-3196

Ge SX, Jung D, Yao R. (2020) ShinyGO: a graphical gene-set enrichment tool for animals and plants. Bioinformatics 36(8): 2628-2629

Gibbs DJ, Lee SC, Isa NM, Gramuglia S, Fukao T, Bassel GW, Correia CS, Corbineau F, Theodoulou FL, Bailey-Serres J, et al. (2011) Homeostatic response to hypoxia is regulated by the N-end rule pathway in plants. Nature 479: 415-418

Gibbs DJ, Md Isa N, Movahedi M, Lozano-Juste J, Mendiondo GM, Berckhan S, Marín-de la Rosa N, Vicente Conde J, Sousa Correia C, Pearce SP. et al. (2014) Nitric oxide sensing in plants is mediated by proteolytic control of group VII ERF transcription factors. Mol. Cell. 53: 369-379

Gibbs DJ, Tedds HM, Labandera AM, Bailey M, White MD, Hartman S, Sprigg C, Mogg SL, Osborne R, Dambire C, et al, (2018) Oxygen-dependent proteolysis

regulates the stability of angiosperm polycomb repressive complex 2 subunit VERNALIZATION 2. Nat. Commun. 9: 5438

Gil P, Dewey E, Friml J, Zhao Y, Snowden KC, Putterill J, Palme K, Estelle M, Chory J. (2001) BIG: a calossin-like protein required for polar auxin transport in Arabidopsis. Genes Dev. 15: 1985-1997

Giuntoli B, Shukla V, Maggiorelli F, Giorgi FM, Lombardi L, Perata P, Licausi F (2017) Age-dependent regulation of ERF-VII transcription factor activity in *Arabidopsis thaliana*. Plant Cell Environ. 40: 2333-2346

Graciet E, Mesiti F, Wellmer F, (2010) Structure and evolutionary conservation of the plant N-end rule pathway. Plant J. 61: 741-751

Graciet E, Walter F, Ó'Maoiléidigh DS, Pollmann S, Meyerowitz EM, Varshavsky A, Wellmer F. (2009) The N-end rule pathway controls multiple functions during Arabidopsis shoot and leaf development. Proc. Natl. Acad. Sci. U. S. A. 10: 13618-13623

Gravot A, Richard G, Lime T, Lemarié S, Jubault M, Lariagon C, Lemoine J, Vicente J, Robert-Seilaniantz A, Holdsworth MJ, et al. (2016). Hypoxia response in Arabidopsis roots infected by *Plasmodiophora brassicae* supports the development of clubroot. BMC Plant Biol. 16: 251

Guo X, Lu W, Ma Y, Qin Q, Hou S. (2013) The *BIG* gene is required for auxin-mediated organ growth in Arabidopsis. Planta 237: 1135-1147

Hartman S, Liu Z, van Veen H, Vicente J, Reinen E, Martopawiro S, Zhang H, van Dongen N, Bosman F, Bassel GW, et al. (2019) Ethylene-mediated nitric oxide depletion pre-adapts plants to hypoxia stress. Nat. Commun. 10: 4020

He J, Zhang RX, Peng K, Tagliavia C, Li S, Xue S, Liu A, Hu H, Zhang J, Hubbard KE, et al. (2018) The BIG protein distinguishes the process of CO_2-induced stomatal closure from the inhibition of stomatal opening by CO_2. New Phytol. 218: 232-241

Hearn TJ, Marti Ruiz MC, Abdul-Awal SM, Wimalasekera R, Stanton CR, Haydon MJ, Theodoulou FL, Hannah MA, Webb AAR. (2018) *BIG* Regulates Dynamic Adjustment of Circadian Period in *Arabidopsis thaliana*. Plant Physiol. 178: 358-371

Holdsworth MJ, Vicente J, Sharma G, Abbas M, Zubrycka A. (2020) The plant N-degron pathways of ubiquitin-mediated proteolysis. J. Integr. Plant. Biol. 62: 70-89

Holman TJ, Jones PD, Russell L, Medhurst A, Ubeda Tomás S, Talloji P, Marquez J, Schmuths H, Tung SA, Taylor I, et al. (2009) The N-end rule pathway promotes seed germination and establishment through removal of ABA sensitivity in Arabidopsis. Proc. Natl. Acad. Sci. U. S. A. 106: 4549-4554

Hong, J.H., Kaustov, L., Couadu, E., Srikumar, T., Wan, J., Arrowshmith, C., Raught, B. (2015) KCMF1 (potassium channel modulatory factor 1) links RAD6 to UBR5 (ubiquitin N-recognin domain-containing E3 ligase 4) and lysosome-mediated degradation. Mol. Cell. Proteom. 14.3 674-685

Hunt LC, Stover J, Haugen B, Shaw TI, Li Y, Pagala VR, Finkelstein D, Barton ER, Fan Y, Labelle M, et al. (2019) A Key Role for the Ubiquitin Ligase UBR4 in Myofiber Hypertrophy in Drosophila and Mice. Cell Rep. 28: 1268-1281

Hunt LC, Schadeberg B, Stover J, Haugen B, Pagala V, Wang YD, Puglise J, Barton ER, Peng J, Demontis F. (2021) Antagonistic control of myofiber size and muscle protein quality control by the ubiquitin ligase UBR4 during aging. Nat Commun. 12: 1418.

Hwang CS, Shemorry A, Auerbach D, Varshavsky A. (2010) The N-end rule pathway is mediated by a complex of the RING-type Ubr1 and HECT-type Ufd4 ubiquitin ligases. Nat. Cell Biol. 12: 1177–1185

Ivanova A, Law SR, Narsai R, Duncan O, Lee JH, Zhang B, Van Aken O, Radomiljac JD, van der Merwe M, Yi, J et al. (2014) A Functional Antagonistic Relationship between Auxin and Mitochondrial Retrograde Signaling Regulates Alternative Oxidase1a Expression in Arabidopsis. Plant Physiol. 165: 1233-1254

Jeong DE, Lee HS, Ku B, Kim CH, Kim SJ, Shin HC. (2023) Insights into the recognition mechanism in the UBR box of UBR4 for its specific substrates. Commun Biol. 6: 1214.

Kannt A, Đikić I. (2021) Expanding the arsenal of E3 ubiquitin ligases for proximity-induced protein degradation. Cell Chem. Biol. 28: 1014-1031

Kanyuka K, Praekelt U, Franklin KA, Billingham OE, Hooley R, Whitelam GC, Halliday KJ. (2003) Mutations in the huge Arabidopsis gene *BIG* affect a range of hormone and light responses. Plant J. 35: 57-70

Kasajima I, Ohkama-Ohtsu N, Ide Y, Haysashi H, Yoneyama T, Suzuki Y, Naito S, Fujiwara T. (2007) The *BIG* gene is involved in regulation of sulfur deficiency-responsive genes in *Arabidopsis thaliana*. Physiol. Plant. 129: 351-363

Kim JG, Shin HC, Seo T, Nawale L, Han G, Kim BY, Kim SJ, Cha- Molstad H. (2021) Signaling Pathways Regulated by UBR Box-Containing E3 Ligases. Int. J. Mol. Sci. 22(15): 8323

Kim L, Kwon DH, Heo J, Park MR, Song HK. (2020) Use of the LC3B-fusion technique for biochemical and structural studies of proteins involved in the N-degron pathway J. Biol. Chem. 295(9): 2590-2600

Kim L, Lin C-C, Lin T-J, Cao Y-C, Chen M-C, Chou M-Y, Lin W-H, Kim M, Wu J-L, Shih M.-C, et al. (2022) Structural analyses of the plant PRT6-UBR box in the Cys-Arg/N-degron pathway and insights into the plant submergence response bioRxiv doi: 10.1101/2022.08.19.504472

Kim ST, Lee YJ, Tasaki T, Mun SR, Hwang J, Kang MJ, Ganipisetti S, Yi EC, Kim BY, Kwon YT. (2018) The N-recognin UBR4 of the N-end rule pathway is targeted to and required for the biogenesis of the early endosome. J Cell Sci. 131. pii: jcs217646.

Kozlic A, Winter N, Telser T, Reimann J, Rose K, Nehlin L, Berckhan S, Sharma G, Dambire C, Boeckx T, et al. (2022) A yeast-based functional assay to study plant N-degron – N-recognin interactions. Front. Plant Sci. 12: 806129. DOI: 10.3389/fpls.2021.806129

Labandera AM, Tedds HM, Bailey M, Sprigg C, Etherington RD, Akintewe O, Kalleechurn G, Holdsworth MJ, Gibbs D. (2021) The PRT6 N-degron pathway restricts VERNALIZATION 2 to endogenous hypoxic niches to modulate plant development. New Phytol. 229: 126-139

Lamichhane S, Alpuerto JB, Han A, Fukao T. (2020) The Central Negative Regulator of Flooding Tolerance, the PROTEOLYSIS 6 Branch of the N-degron Pathway, Adversely Modulates Salinity Tolerance in Arabidopsis. Plants (Basel) 9(11): 1415

Lee SC, Mustroph A, Sasidharan R, Vashisht D, Pedersen O, Oosumi T, Voesenek LA, Bailey-Serres J. (2011) Molecular characterization of the submergence response of the *Arabidopsis thaliana* ecotype Columbia. New Phytol. 190(2): 457-471

Li HM, Altschmied L, Chory J. (1994) Arabidopsis mutants define downstream branches in the phototransduction pathway. Genes Dev. 8: 339-349

Li-Beisson Y, Shorrosh B, Beisson F, Andersson M, Arondel V, Bates P, Baud S, Bird D, DeBono A, Durrett T, et al. (2013) Acyl-Lipid Metabolism in The Arabidopsis Book, Rockville, MD: American Society of Plant Biologists

Licausi F, Kosmacz M, Weits DA, Giuntoli B, Giorgi FM, Voesenek LA, Perata P, van Dongen JT. (2011) Oxygen sensing in plants is mediated by an N-end rule pathway for protein destabilization. Nature 479: 419-422

Licausi F, van Dongen JT, Giuntoli B, Novi G, Santaniello A, Geigenberger P, Perata P.(2010) HRE1 and HRE2, two hypoxia-inducible ethylene response factors, affect anaerobic responses in Arabidopsis thaliana. Plant J. 62: 302-315

Lichtenthaler HK, Wellburn AR. (1983) Determination of Total Carotenoids and Chlorophyll a and b of Leaf Extracts in Different Solvents. Biochemical Society Transactions, 603: 591-603

Lin R, Tao R, Gao X, Li T, Zhou X, Guan KL, Xiong Y, Lei QY. (2013) Acetylation stabilizes ATP-citrate lyase to promote lipid biosynthesis and tumor growth. Mol Cell. 2013 Aug 22;51(4):506-518.

Linden KJ, Callis J. (2020) The ubiquitin system affects agronomic plant traits. J. Biol. Chem. 295: 13940-13955

Liu Z, Zhang RX, Duan W, Xue B, Pan X, Li S, Sun P, Pi L, Liang YK. (2022) BIG Modulates Stem Cell Niche and Meristem Development via SCR/SHR Pathway in Arabidopsis Roots. Int. J. Mol. Sci. 23(12): 6784

Livak KJ and Schmittgen TD. (2001) Analysis of relative gene expression data using real-time quantitative PCR and the 2−ΔΔCT method. Methods 25: 402-408

López-Bucio J, Hernández-Abreu E, Sánchez-Calderón L, Pérez-Torres A, Rampey RA, Bartel B, Herrera-Estrella L. (2005) An auxin transport independent pathway is involved in phosphate stress-induced root architectural alterations in Arabidopsis. Identification of *BIG* as a mediator of auxin in pericycle cell activation. Plant Physiol. 137: 681-691

Lou S, Guo X, Liu L, Song Y, Zhang L, Jiang Y, Zhang L, Sun P, Liu B, Tong S, et al. (2022) Allelic shift in cis-elements of the transcription factor RAP2.12 underlies adaptation associated with humidity in Arabidopsis thaliana. Sci. Adv. eabn8281

Luehrsen KR, de Wet JR, Walbot V. (1992) Transient expression analysis in plants using firefly luciferase reporter gene. Meths. Enzymol. 216: 397-414

Mair A, Xu SL, Branon TC, Ting AY, Bergmann DC. (2019) Proximity labeling of protein complexes and cell-type-specific organellar proteomes in Arabidopsis enabled by TurboID. Elife 8: e47864

Masson N, Keeley TP, Giuntoli B, White MD, Puerta ML, Perata P, Hopkinson RJ, Flashman E, Licausi F, Ratcliffe PJ (2019) Conserved N-terminal cysteine dioxygenases transduce responses to hypoxia in animals and plants. Science. 365: 65-69

Mendiondo GM, Gibbs DJ, Szurman-Zubrzycka M, Korn A, Marquez J, Szarejko I, Maluszynski M, King J, Axcell B, Smart K, et al. (2016) Enhanced waterlogging tolerance in barley by manipulation of expression of the N-end rule pathway E3 ligase PROTEOLYSIS6. Plant Biotechnol. J. 14: 40-50

Meteignier LV, El Oirdi M, Cohen M, Barff T, Matteau D, Lucier JF, Rodrigue S, Jacques PE, Yoshioka K, Moffett P. (2017) Translatome analysis of an NB-LRR immune response identifies important contributors to plant immunity in Arabidopsis. J. Exp. Bot. 68: 2333-2344

Modrego A, Pasternak T, Omary M, Albacete A, Cano A, Pérez-Pérez JM, Efroni I. (2023) Mapping of the Classical Mutation rosette Highlights a Role for Calcium in Wound-Induced Rooting. Plant Cell Physiol. 64(2): 152-164

Mot AC, Prell E, Klecker M, Naumann C, Faden F, Westermann B, Dissmeyer N (2018) Real-time detection of N-end rule-mediated ubiquitination via fluorescently labeled substrate probes. New Phytol. 217: 613-624

Mustroph A, Bailey-Serres J. (2010) The Arabidopsis translatome cell-specific mRNA atlas: Mining suberin and cutin lipid monomer biosynthesis genes as an example for data application. Plant Signal Behav. 5: 320-324

Mustroph A, Zanetti ME, Jang CJ, Holtan HE, Repetti PP, Galbraith DW, Girke T, Bailey-Serres J. (2009) Profiling translatomes of discrete cell populations resolves

altered cellular priorities during hypoxia in Arabidopsis. Proc. Natl. Acad. Sci. U. S. A. 106(44): 18843-18848

Perez-Riverol Y, Bai J, Bandla C, Hewapathirana S, García-Seisdedos D, Kamatchinathan S, Kundu D, Prakash A, Frericks-Zipper A, Eisenacher M, et al. (2022) The PRIDE database resources in 2022: A Hub for mass spectrometry-based proteomics evidences. Nucleic Acids Res. 50: D543-D552

Potuschak T, Stary S, Schlögelhofer P, Becker F, Nejinskaia V, Bachmair A. (1998) PRT1 of *Arabidopsis thaliana* encodes a component of the plant N-end rule pathway. Proc. Natl. Acad. Sci. U. S. A. 95: 7904-7908

Rappsilber J, Mann M, Ishihama Y. (2007) Protocol for micro-purification, enrichment, pre-fractionation and storage of peptides for proteomics using StageTips. Nat. Protoc. 2: 1896-906

Riber W, Müller JT, Visser EJ, Sasidharan R, Voesenek LA, Mustroph A. (2015).The *greening after extended darkness1* is an N-end rule pathway mutant with high tolerance to submergence and starvation. Plant Physiol. 167(4): 1616-29

Ritchie ME, Phipson B, Wu D, Hu Y, Law CW, Shi W, Smyth GK. (2015) Limma powers differential expression analyses for RNA-sequencing and microarray studies. Nucleic Acids Res. 43; e47

Ruegger M, Dewey E, Hobbie L, Brown D, Bernasconi P, Turner J, Muday G, Estelle M. (1997) Reduced naphthylphthalamic acid binding in the *tir3* mutant of Arabidopsis is associated with a reduction in polar auxin transport and diverse morphological defects. Plant Cell. 9: 745-757

Serra O, Geldner N. (2022) The making of suberin. New Phytol. 235(3): 848-866

Shinohara N, Taylor C, Leyser O. (2013) Strigolactone can promote or inhibit shoot branching by triggering rapid depletion of the auxin efflux protein PIN1 from the plasma membrane. PLoS Biol. 11: e1001474

Shukla V, Han JP, Cléard F, Lefebvre-Legendre L, Gully K, Flis P, Berhin A, Andersen TG, Salt DE, Nawrath C, Barberon M (2021) Suberin plasticity to developmental and exogenous cues is regulated by a set of MYB transcription factors. Proc Natl Acad Sci U S A. 118: e2101730118

Stary S, Yin XJ, Potuschak T, Schlögelhofer P, Nizhynska V, Bachmair A (2003) PRT1 of Arabidopsis is a ubiquitin protein ligase of the plant N-end rule pathway with specificity for aromatic amino-terminal residues. Plant Physiol. 133: 1360-1366

Tanaka T, Tanaka H, Machida C, Watanabe M, Machida Y (2004) A new method for rapid visualization of defects in leaf cuticle reveals five intrinsic patterns of surface defects in Arabidopsis. Plant J. 37:139-146

Tang D, Sandoval W, Lam C, Haley B, Liu P, Xue D, Roy D, Patapoff T, Louie S, Snedecor B, Misaghi S. (2020) UBR E3 ligases and the PDIA3 protease control degradation of unfolded antibody heavy chain by ERAD. J Cell Biol. 219, e201908087.

Tasaki T, Kim ST, Zakrzewska A, Lee BE, Kang MJ, Yoo YD, Cha-Molstad HJ, Hwang J, Soung NK, Sung KS, et al. (2013) UBR box N-recognin-4 (UBR4), an N-recognin of the N-end rule pathway, and its role in yolk sac vascular development and autophagy. Proc. Natl. Acad. Sci. U S A. 110: 3800-3805

Tasaki T, Mulder LCF, Iwamatsu A, Lee MJ, Davydov IV, Varshavsky A, Muesing M, Kwon YT. (2005) A family of mammalian E3 ubiquitin ligases that contain the UBR box motif and recognise N-degrons. Mol. Cell Biol. 25: 7120-7136

Tasaki T, Zakrzewska A, Dudgeon DD, Jiang Y, Lazo JS, Kwon YT. (2009) The substrate recognition domains of the N-end rule pathway. J. Biol. Chem. 284(3): 1884-1895

Theodoulou FL, Orosa-Puente B, Trujillo M, Rubio V. (2022) Plant proteostasis: a proven and promising target for crop improvement. Essays Biochem. 66: 75-85

Till CJ, Vicente J, Zhang H, Oszvald M, Deery MJ, Pastor V, Lilley KS, Ray RV, Theodoulou FL, Holdsworth MJ. (2019) The *Arabidopsis thaliana* N-recognin E3 ligase PROTEOLYSIS1 influences the immune response. Plant Direct 3: e00194

Tyanova S. Temu T. Cox J. (2016) The MaxQuant computational platform for mass spectrometry-based shotgun proteomics. Nat. Protoc. 11: 2301-2319

Ursache R, De Jesus Vieira Teixeira C, Dénervaud Tendon V, Gully K, De Bellis D, Schmid-Siegert E, Grube Andersen T, Shekhar V, Calderon S, Pradervand S, et al. (2021) GDSL-domain proteins have key roles in suberin polymerization and degradation. Nat. Plants. 7: 353-364

Üstün S, Sheikh A, Gimenez-Ibanez S, Jones A, Ntoukakis V, Börnke F. (2016) The Proteasome Acts as a Hub for Plant Immunity and Is Targeted by Pseudomonas Type III Effectors. Plant Physiol. 172: 1941-1958

Varshavsky A. (2000) Ubiquitin fusion technique and its descendants. Methods Enzymol. 327: 578–593

Varshavsky A. (2019) N-degron and C-degron pathways of protein degradation. Proc. Natl. Acad. Sci. U S A 116: 358-366

Vicente J, Mendiondo GM, Movahedi M, Peirats-Llobet M, Juan YT, Shen YY, Dambire C, Smart K, Rodriguez PL, Charng YY, et al. (2017) The Cys-Arg/N-End Rule Pathway Is a General Sensor of Abiotic Stress in Flowering Plants. Curr. Biol. 27: 3183-3190.e4

Vicente J, Mendiondo GM, Pauwels J, Pastor V, Izquierdo Y, Naumann C, Movahedi M, Rooney D, Gibbs DJ, Smart K, et al. (2019) Distinct branches of the N-end rule pathway modulate the plant immune response. New Phytol. 221: 988-1000

Wang K, Froehlich JE, Zienkiewicz A, Hersh HL, Benning C (2017) A Plastid Phosphatidylglycerol Lipase Contributes to the Export of Acyl Groups from Plastids for Seed Oil Biosynthesis. Plant Cell. 29: 1678-1696

Wang Z, Spoel SH. (2022) HECT ubiquitin ligases as accessory proteins of the plant proteasome. Essays Biochem. 66: 135-145

Weits DA, Giuntoli B, Kosmacz M, Parlanti S, Hubberten HM, Riegler H, Hoefgen R, Perata P, van Dongen JT, Licausi F. (2014) Plant cysteine oxidases control the oxygen-dependent branch of the N-end-rule pathway. Nat. Commun. 5: 3425

Weits DA, Kunkowska AB, Kamps NCW, Portz KMS, Packbier NK, Nemec Venza Z, Gaillochet C, Lohmann JU, Pedersen O, van Dongen JT, et al. (2019) An apical hypoxic niche sets the pace of shoot meristem activity. Nature 569(7758): 714-717

Weits DA, Zhou L, Giuntoli B, Carbonare LD, Iacopino S, Piccinini L, Lombardi L, Shukla V, Bui LT, Novi G, van Dongen JT, Licausi F (2023) Acquisition of hypoxia inducibility by oxygen sensing N-terminal cysteine oxidase in spermatophytes. Plant Cell Environ. 46: 322-338

White MD, Klecker M, Hopkinson RJ, Weits DA, Mueller C, Naumann C, O'Neill R, Wickens J, Yang J, Brooks-Bartlett JC, et al. (2017) Plant cysteine oxidases are

dioxygenases that directly enable arginyl transferase-catalysed arginylation of N-end rule targets. Nat. Commun. 8: 14690

Worley CK, Ling R, Callis J. (1998) Engineering in vivo instability of firefly luciferase and Escherichia coli beta-glucuronidase in higher plants using recognition elements from the ubiquitin pathway. Plant Mol. Biol. 37: 337–347

Wu L, Luo P, Di DW, Wang L, Wang M, Lu CK, Wei SD, Zhang L, Zhang TZ, Amakorová P, et al. (2015) Forward genetic screen for auxin-deficient mutants by cytokinin. Sci. Rep. 5: 11923

Xie Y, Varshavsky YA. (2000) Physical association of ubiquitin ligases and the 26S proteasome. Proc. Natl. Acad. Sci. U. S. A. 97: 2497-502

Xu H, Liu P, Wang C, Wu S, Dong C, Lin Q, Sun W, Huang B, Xu M, Tauqeer A, et al. (2022) Transcriptional networks regulating suberin and lignin in endodermis link development and ABA response. Plant Physiol. 190(2): 1165-1181

Yamaguchi N, Komeda Y. (2013) The role of CORYMBOSA1/BIG and auxin in the growth of Arabidopsis pedicel and internode. Plant Sci. 209: 64-74

Yamaguchi N, Suzuki M, Fukaki H, Morita-Terao M, Tasaka M, Komeda Y. (2007) *CRM1/BIG*-mediated auxin action regulates Arabidopsis inflorescence development. Plant Cell Physiol. 48: 1275-1290

Yau RG, Doerner K, Castellanos ER, Haakonsen DL, Werner A, Wang N, Yang XW, Martinez-Martin N, Matsumoto ML, Dixit VM, et al. (2017) Assembly and Function of Heterotypic Ubiquitin Chains in Cell-Cycle and Protein Quality Control. Cell. 171, 918-933.e20

Yoo YD, Mun SR, Ji CH, Sung KW, Kang KY, Heo AJ, Lee SH, An JY, Hwang J, Xie XQ, et al. (2018) N-terminal arginylation generates a bimodal degron that modulates autophagic proteolysis. Proc. Natl. Acad. Sci. U. S. A. 115: E2716-E2724

Yoshida S, Ito M, Callis J, Nishida I, Watanabe A. (2002) A delayed leaf senescence mutant is defective in arginyl-tRNA:protein arginyltransferase, a component of the N-end rule pathway in Arabidopsis. Plant J. 32(1): 129-37

Zhang H, Gannon L, Hassall KL, Deery MJ, Gibbs DJ, Holdsworth MJ, van der Hoorn RAL, Lilley KS, Theodoulou FL. (2018a) N-terminomics reveals control of

Arabidopsis seed storage proteins and proteases by the Arg/N-end rule pathway. New Phytol. 218: 1106-1126

Zhang H, Gannon L, Jones PD, Rundle CA, Hassall KL, Gibbs DJ, Holdsworth MJ, Theodoulou FL. (2018b) Genetic interactions between ABA signalling and the Arg/N-end rule pathway during Arabidopsis seedling establishment. Sci. Rep. 8: 15192

Zhang RX, Ge S, He J, Li S, Hao Y, Du H, Liu Z, Cheng R, Feng YQ, Xiong L, et al. (2019a) *BIG* regulates stomatal immunity and jasmonate production in Arabidopsis. New Phytol. 222: 335-348

Zhang RX, Li S, He J, Liang YK. (2019b) *BIG* regulates sugar response and C/N balance in Arabidopsis. Plant Signal Behav. 14: 1669418

Zhang WJ, Zhai LM, Yu HX, Peng J, Wang SS, Zhang XS, Su YH, Tang LP. (2020) The *BIG* gene controls size of shoot apical meristems in *Arabidopsis thaliana*. Plant Cell Rep. 39: 543-552

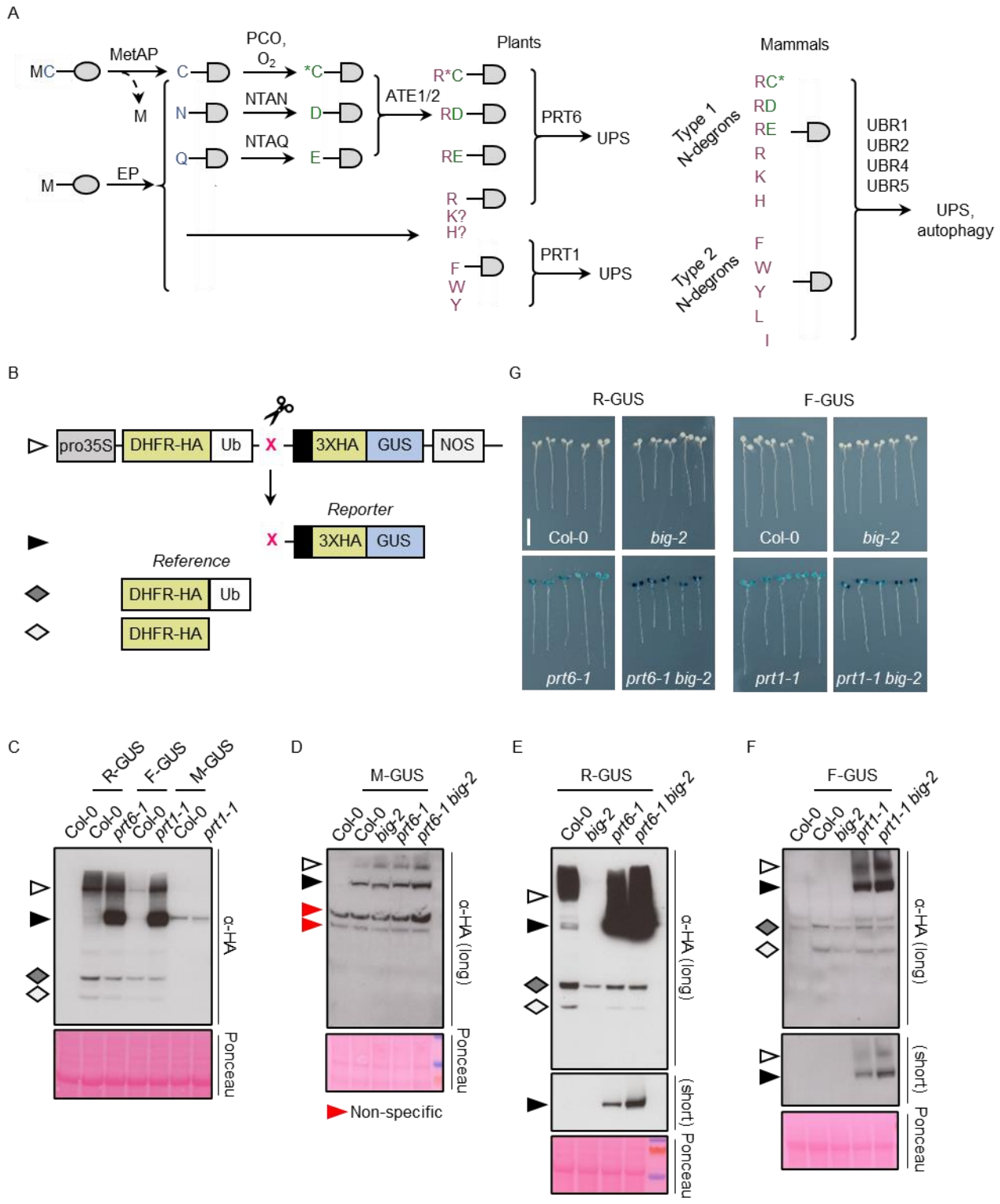

Figure 1. BIG influences the stability of model type 1 and type 2 Arg/N-degron pathway substrates.

(A) Schematic showing the architecture of the Arg/N-degron pathway and specificity of N-recognins in plants and mammals. Single letter codes for amino acid residues are used; *C indicates oxidised cysteine. Proteins (represented by grey ovals) may become N-degron pathway substrates via cleavage by non-processive endopeptidases (EP), or by methionine aminopeptidase (MetAP), where the second residue is small. Substrates may also be generated by enzymatic modification of N-termini by PLANT CYSTEINE OXIDASE (PCO), Asn-specific N-terminal amidase (NTAN), Gln-specific N-

terminal amidase (NTAQ), and arginyl-tRNA protein transferase (ATE). In plants, destabilising residues thus generated are targeted for degradation by the Ubiquitin Proteasome System (UPS) via N-recognin E3 ligases PROTEOLYSIS6 (PRT6; specific for basic N-termini) and PROTEOLYSIS1 (PRT1; specific for aromatic N-termini). In mammals, four N-recognins act semi-redundantly to mediate the degradation of both type 1 and type 2 substrates via the UPS or by autophagy. (B) Generation of N-degron pathway X-GUS substrates. Constructs driven by the constitutive *CaMV35S* promoter (Pro35S) encode a fusion of mouse dihydrofolate reductase (DHFR, yellow) to ubiquitin (variant K48R; Ub, white), followed by *Escherichia coli* beta glucuronidase (GUS, blue). Ubiquitin-specific proteases (indicated by the scissors icon) remove ubiquitin co-translationally to release the GUS reporter protein and reveal a new N terminus (residue of choice, X). The GUS ORF is extended by unstructured amino acids (black) to enhance the effect of destabilising amino-terminal residues. The cleavage also creates a stable DHFR reference protein and HA epitopes enable immunological detection of both products (Garzón et al., 2007). NOS, nopaline synthase terminator. Note that the stable reference carries one copy of the HA epitope, whereas the reporter has three copies. (C-F) Detection of N-degron pathway substrates by immunoblotting of crude protein extracts from 6-d old seedlings of different genotypes expressing X-GUS reporters. Symbols to the left indicate the protein products shown in (B). Blots were developed until the stable reference protein could be detected (α-HA long); where the stabilised reporter band signal is saturated, a shorter exposure is shown in the lower panel (short) for clarity. Ponceau S staining was used to confirm equal loading. (G) Histochemical staining of GUS reporter activity in 6-d old seedlings expressing R-GUS and F-GUS test substrates. Representative seedlings were rearranged on an agar plate, prior to photography. Bar, 1 cm (images are scaled identically).

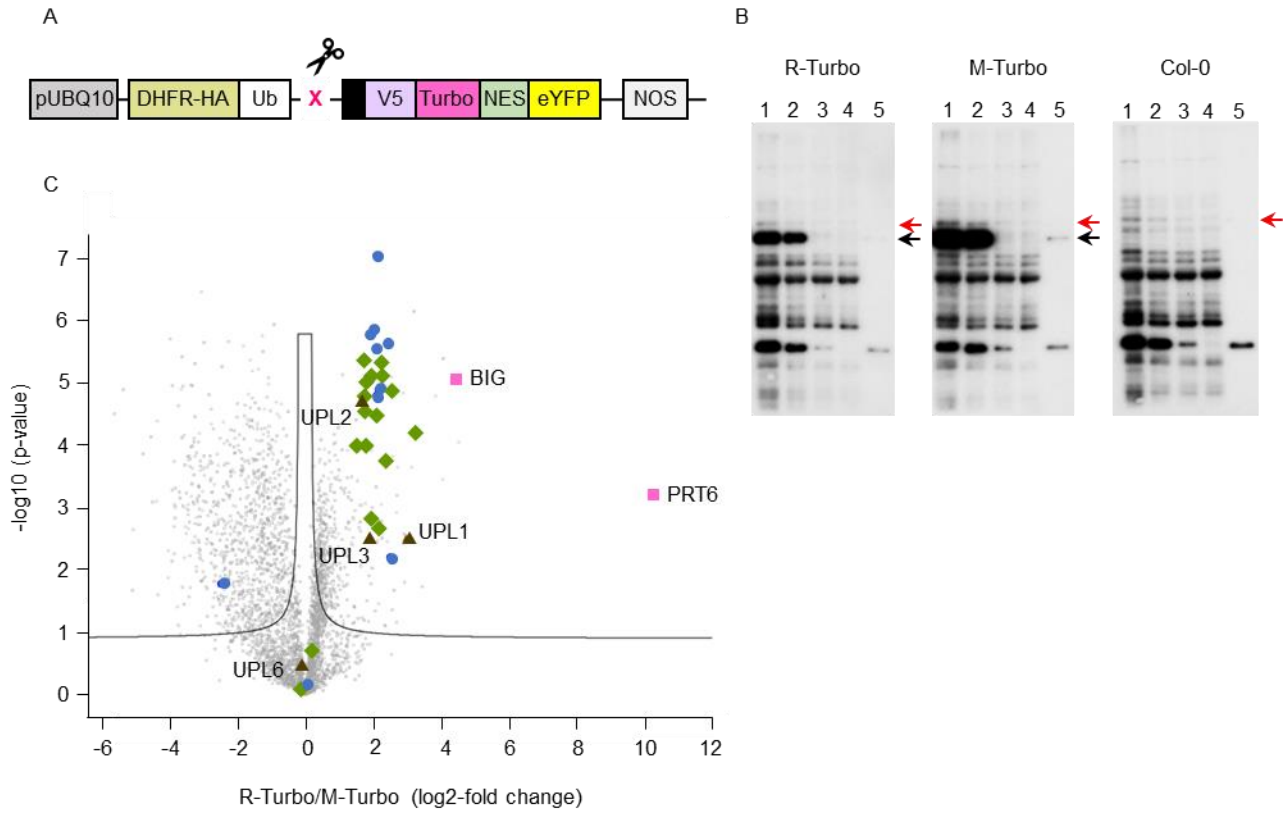

Figure 2. Identification of N-degron proximal proteins

(A) Schematic of construct used for proximity labelling assay. Turbo-NES-eYFP (Mair et al., 2019) was modified to harbour an N-terminal ubiquitin (Ub) fusion construct, comprising dihydrofolate reductase-HA epitope-Ub (DHFR-HA-Ub) followed by the N-terminal amino acid of choice (X) in front of a fusion comprising a linker sequence (black), the V5 epitope, modified *Escherichia coli* biotin ligase (Turbo), a nuclear export signal (NES) and enhanced yellow fluorescent protein (eYFP). The construct was expressed from the *POLYUBIQUITIN10* promoter (ProUBQ10). The fusion protein is cleaved in planta by ubiquitin specific proteases, indicated by the scissors icon. (B) Anti-biotin immunoblots to follow the enrichment of biotinylated protein in extracts from 7-d old Col-0 and plants expressing R-Turbo and M-Turbo. Lane 1, crude extract; lane 2, extract after desalting; lanes 3 and 4, supernatant after two subsequent incubations with streptavidin beads (unbound fractions); lane 5, streptavidin beads after first incubation. Black arrows indicate the bait proteins R-Turbo and M-Turbo (70.2 kDa), and the red arrow indicates a non-specific background band. (C) Volcano plot visualising enrichment of biotinylated proteins when comparing transgenic lines expressing R-Turbo versus M-Turbo, after proteasome inhibition to ensure equal presence of either protein. PRT6 and BIG (magenta squares) are the two most enriched proteins. Olive diamonds, non-ATPase subunits of the proteasome; blue circles, ATPase subunits; brown triangles, Homologous to the E6-AP Carboxyl Terminus (HECT) E3 ubiquitin ligases.

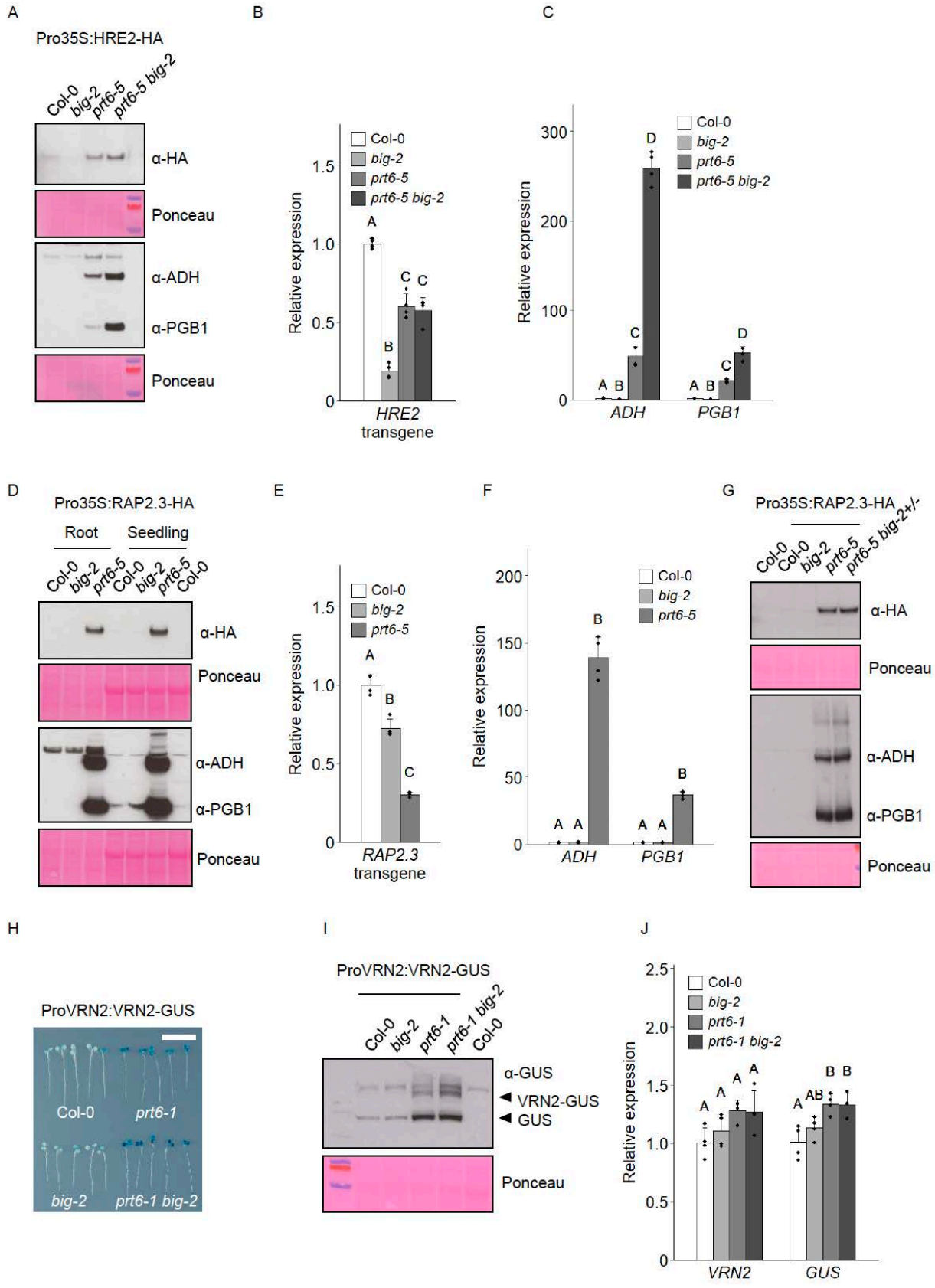

Figure 3. BIG influences the abundance of physiological PRT6/N-degron pathway substrates.

(A-C) Molecular analysis of seedlings expressing Pro35S:HRE2-HA. (A) Immunoblots of crude protein extracts from 6-d old roots of the indicated genotypes, probed with anti-HA (α-HA) antiserum or antibodies specific for the hypoxia markers, alcohol dehydrogenase (ADH) and phytoglobin1 (PGB1; the hypoxia marker antibodies were applied simultaneously to a single membrane). Ponceau S staining was used to confirm equal loading. (B) Expression of *HRE2* transgene relative to Col-0. Values are means ± SD (n=4). (C) Expression of *ADH* and *PGB1* relative to Col-0. Values are means ± SD (n=4). (D-G) Molecular analysis of seedlings expressing Pro35S:RAP2.3-HA. (D, G) Immunoblots of crude protein extracts from 6-d old seedlings of the indicated genotypes, probed with anti-HA (α-HA) antiserum or antibodies specific for the hypoxia markers, ADH and PGB1. (E) Expression of *RAP2.3* transgene relative to Col-0. Values are means ± SD (n=4). (F) Expression of *ADH* and *PGB1* relative to Col-0. Values are means ± SD (n=4). (H-J) Molecular analysis of seedlings expressing ProVRN2:VRN2-GUS. (H) Histochemical staining of glucuronidase (GUS) reporter activity in 6-d old seedlings. Seedlings were rearranged on an agar plate prior to photography. Bar, 1 cm. (I) Immunoblot of 6-d old seedlings probed with anti-GUS antibody. (J) Expression of *VRN2* and *GUS* relative to Col-0. Values are means ± SD (n=4). For all plots, different letters indicate significant differences between conditions ($P < 0.05$; ANOVA with Tukey multiple comparison test).

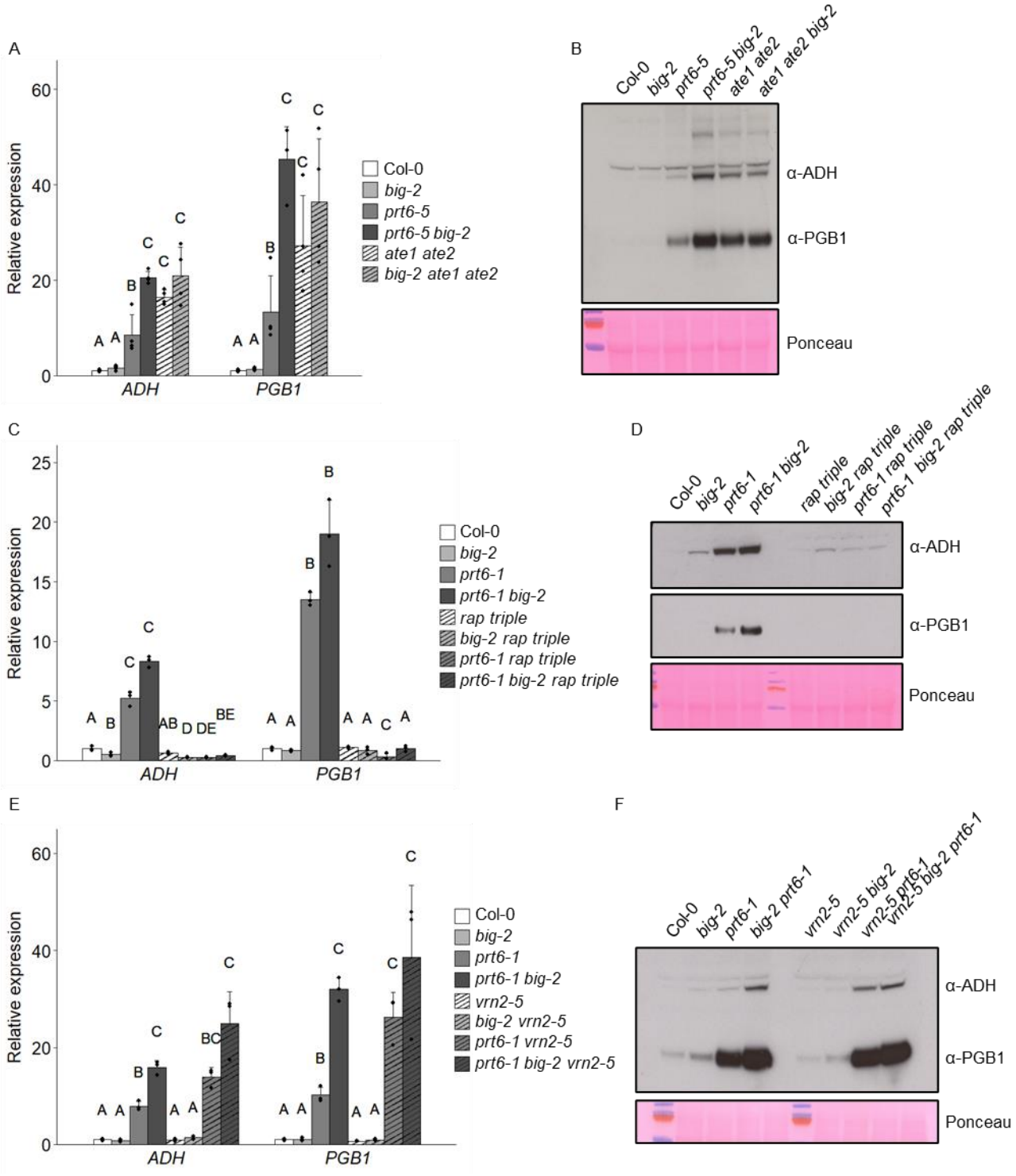

Figure 4. Regulation of the hypoxia response by BIG requires ATE1/2 and ERFVIIs

(A,B) Molecular analysis of PRT6/N-degron pathway mutants. (A) Expression of *ADH* and *PGB1* relative to Col-0 in 6-d old seedlings. Values are means ± SD (n=4). (B) Immunoblots of crude protein extracts from 6-d old seedlings of the indicated genotypes, probed with antibodies specific for the hypoxia markers, alcohol dehydrogenase (ADH) and phytoglobin1 (PGB1) (which were applied to the same membrane). (C-F) Molecular analysis of PRT6/N-degron pathway mutants combined with *rap2.12 rap2.2 rap2.3* mutant alleles ("*rap triple*") (C,D) or with *vrn2-5* (E,F). (C,E) Expression of *ADH* and *PGB1* relative to Col-0 in 6-d old seedlings. Values are means ± SD (n=3). (D,F) Immunoblot of crude protein extracts from 6-d old seedlings of the indicated genotypes, probed with anti-HA (α-HA)

antiserum or antibodies specific for the hypoxia markers, ADH and PGB1. Ponceau S staining was used to confirm equal loading. For all plots, different letters indicate significant differences between conditions ($P < 0.05$; ANOVA with Tukey multiple comparison test).

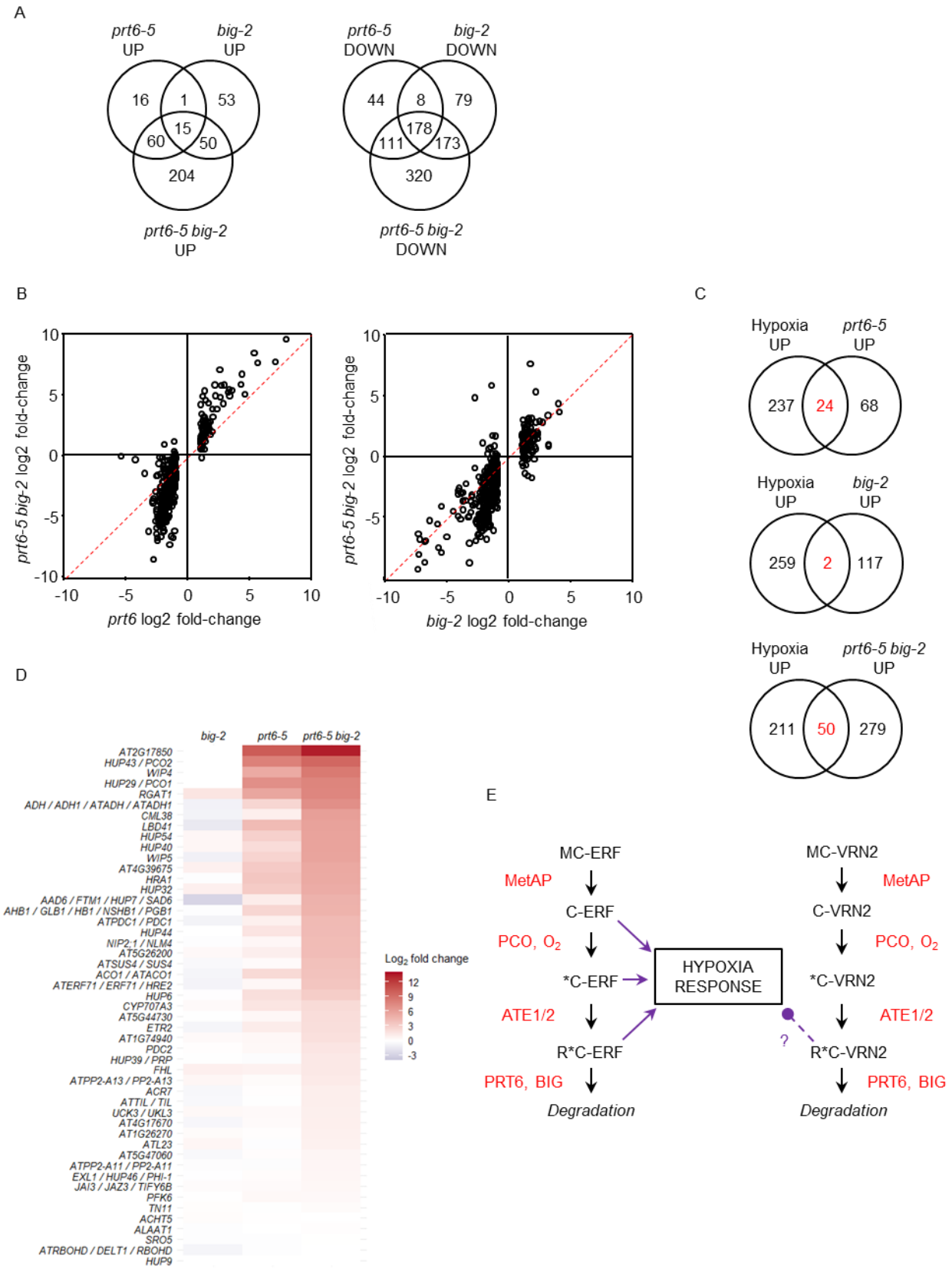

Figure 5. Impact of BIG on the root transcriptome

(A) Numbers of differentially expressed genes (DEGs) in roots of different mutant backgrounds. DEGs are defined as having a fold change greater than or equal to two at adjusted p-value<0.01. (B) Plots comparing the fold-change of transcripts in *big-2* and *prt6-5* single mutants with the double mutant,

prt6-5 big-2. The dashed red line indicates equal fold change in the two genotypes. (C) Venn diagram showing overlap of DEGs with hypoxia responsive genes in Arabidopsis roots (differentially regulated following 7h of dark submergence; Lee et al., 2011), indicated in red. (D) Heatmap showing log2 fold change of 49 “core hypoxia” genes (Mustroph et al., 2009) in the different mutant backgrounds relative to Col-0. Red and blue indicate up and down regulated genes, respectively. Gene names or AGI codes are shown to the left of the panel. (E) Scheme summarising impact of BIG on the N-degron pathway and the hypoxia response. Under normoxia, ERVII transcription factors and VRN2 are sequentially modified by methionine aminopeptidases (MetAP), plant cysteine oxidases (PCO) and arginyl-tRNA protein transferases (ATE1/2), such that the Nt Met is removed to reveal Cys2, which is oxidised (*C) and then arginylated (R*C). R*C-ERF and R*C-VRN2 are then targeted for degradation by PRT6 and also by a process involving BIG. Degradation is prevented in hypoxic conditions and in the absence of PRT6 (and BIG) function. The accumulation of ERFVIIs initiates the transcription of hypoxia responsive genes. The accumulation of VRN2 negatively influences the expression of certain hypoxia responsive genes.

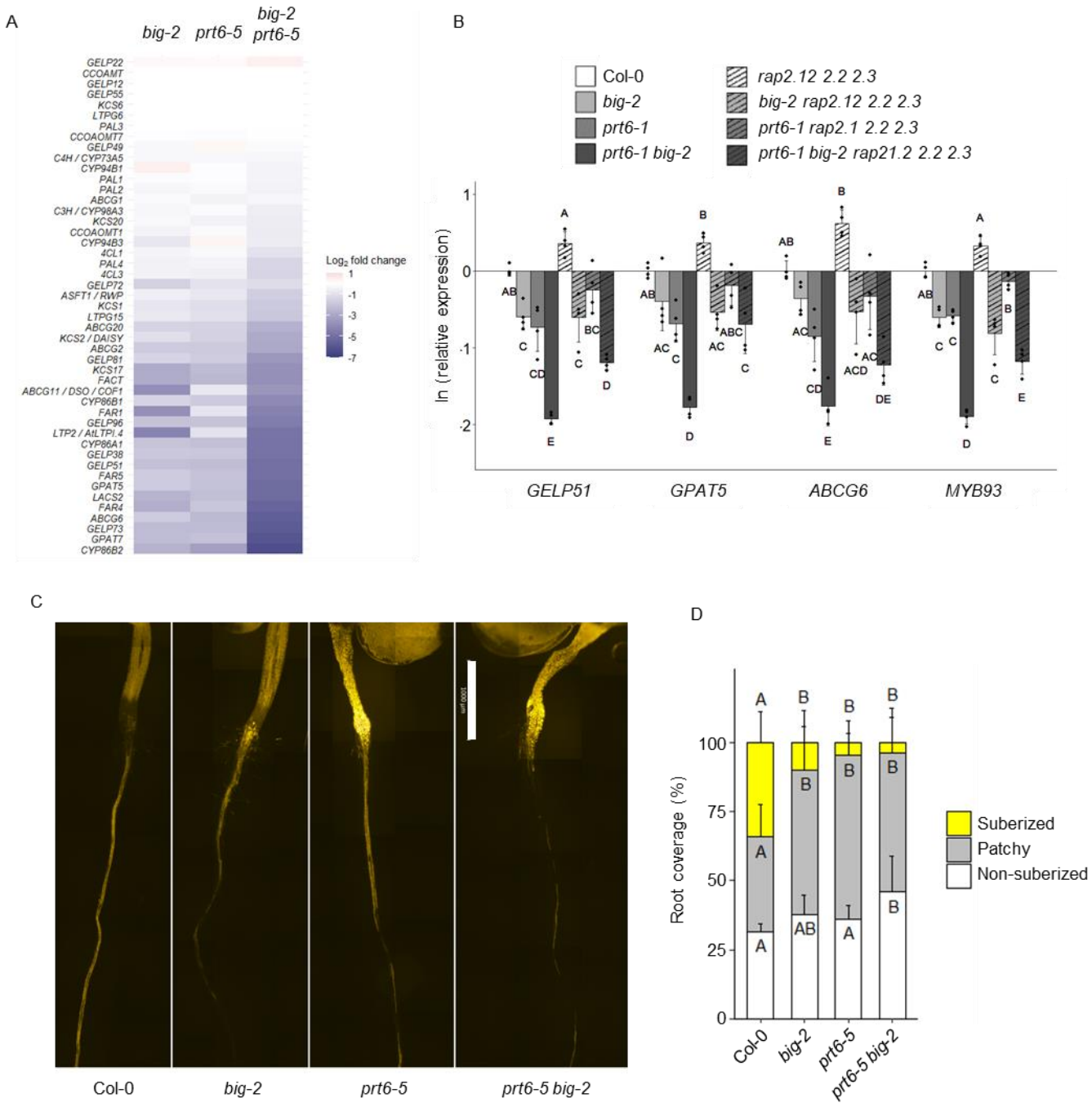

Figure 6. PRT6 and BIG regulate suberin deposition in roots

(A) Heatmap derived from RNA-seq data showing log2 fold change of genes associated with suberin biosynthesis and deposition in the different mutant backgrounds, relative to Col-0. The gene list was curated from (Mustroph and Bailey-Serres, 2010; Ursache et al., 2021; Serra and Geldner, 2022). Gene names or AGI codes are shown to the left of the panel. (B) RT-qPCR analysis of genes involved in suberin biosynthesis and deposition in 5-d old roots of mutants, showing natural log of expression relative to Col-0. Values are means ± SD (n=4); different letters indicate significant differences between genotypes ($P < 0.05$). (C) Representative composite micrographs showing Fluorol Yellow 088 staining of suberin in wild type and mutant roots (scale bar represents 1 mm; images are scaled identically). The full root images are shown in Fig. S8. (D) Quantification of suberin deposition along the root axis using three different zones: non-suberized, patchy, and continuous. Data are presented as mean percentage coverage of root length ± SD (n=10 roots; representative of two independent experiments); different letters indicate significant differences between genotypes for each region ($P < 0.05$; ANOVA with Tukey multiple comparison test)

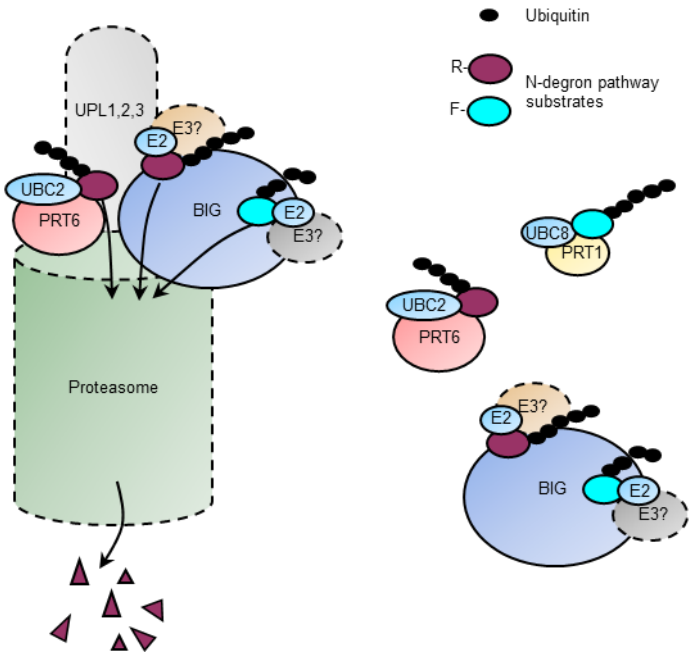

Figure 7. Speculative model for action of PRT6 and BIG

The cartoon is based on information from the literature and data from the current study. A subset of the cellular pool of BIG and PRT6 is bound to the proteasome lid where the two proteins may interact (Xie & Varshavsky, 2000; Besche et al., 2009; 2014; Űstün et al., 2016; Fig. 2), but BIG and PRT6 likely also work without association with the proteasome, as indicated by the dashed lines around the proteasome and associated proteins. PRT6 is a candidate E3 ligase that works together with the E2 conjugating enzyme, UBC2 to ubiquitinate protein substrates with basic (type 1) N-termini, targeting them for proteasomal degradation (Garzón et al., 2007; Kozlic et al., 2022). BIG acts as a scaffold, recruiting one or more as-yet unidentified E3 enzymes (indicated by different colours) as well as E2 enzymes to ubiquitinate protein substrates with type 1 and type 2 N-termini, resulting in their degradation (Ashton-Beaucage et al., 2016; Yau et al., 2017; Hunt et al., 2019); Fig. 1E, F). Alternatively, BIG may have intrinsic E3 ligase activity, by analogy with UBR4 (Barnsby-Greer et al., 2024). The PRT1 E3 ligase also mediates degradation of aromatic (type 2) substrates, together with UBC8 (Stary et al., 2003; Mot et al., 2018). Several reports indicate that the HECT-type ubiquitin protein ligases (UPLs) reside at the proteasome, where they increase the processivity of polyubiquitination in concert with multiple E3 ligases (Hwang et al., 2010; Wang and Spoel, 2022).